Cell Reports

Article

ECPAS/Ecm29-mediated 26S proteasome disassembly is an adaptive response to glucose starvation

Graphical abstract

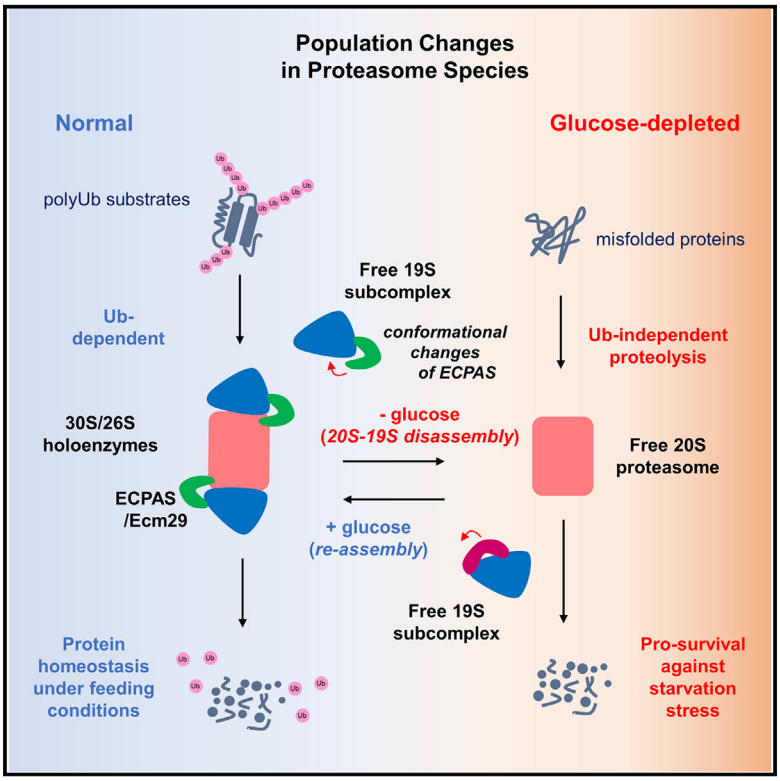

Highlights

- Glucose starvation separates 26S proteasomes into 20S and 19S subcomplexes
- Loss of ECPAS delays 26S disassembly and degradation of 20S proteasome substrates
- ECPAS is essential for ER stress response and cell survival during starvation
- The 26S disassembly is to adapt global proteolysis to physiological needs

Authors

Won Hoon Choi, Yejin Yun, Insuk Byun, ..., Yong Tae Kwon, Michael H. Glickman, Min Jae Lee

Correspondence

glickman@technion.ac.il (M.H.G.), minjlee@snu.ac.kr (M.J.L.)

In brief

Choi et al. show that glucose deprivation induces the separation of 26S proteasomes into 20S and 19S subcomplexes. ECPAS facilitates this process and the breakdown of misfolded proteins in a ubiquitin-independent manner. The alterations in proteasome composition aid cells in adjusting to varying metabolic conditions and counteract proteotoxic stress.

Choi et al., 2023, Cell Reports *42*, 112701
July 25, 2023
https://doi.org/10.1016/j.celrep.2023.112701

CellPress

Cell Reports

CellPress
OPEN ACCESS

Article

ECPAS/Ecm29-mediated 26S proteasome disassembly is an adaptive response to glucose starvation

Won Hoon Choi,[1,9] Yejin Yun,[1,2,9] Insuk Byun,[1,2,9] Sumin Kim,[1,2] Seho Lee,[3] Jiho Sim,[3] Shahar Levi,[4] Seo Hyeong Park,[1,2] Jeongmoo Jun,[1] Oded Kleifeld,[4] Kwang Pyo Kim,[5] Dohyun Han,[6] Tomoki Chiba,[7] Chaok Seok,[3] Yong Tae Kwon,[2,8] Michael H. Glickman,[4,*] and Min Jae Lee[1,2,8,10,*]

[1]Department of Biochemistry and Molecular Biology, Seoul National University College of Medicine, Seoul 03080, Korea
[2]Department of Biomedical Sciences, Seoul National University Graduate School, Seoul 03080, Korea
[3]Department of Chemistry, Seoul National University, Seoul 08826, Korea
[4]Department of Biology, Technion–Israel Institute of Technology, Haifa 32000, Israel
[5]Department of Applied Chemistry, Institute of Natural Science, Global Center for Pharmaceutical Ingredient Materials, Kyung Hee University, Yongin 17104, Korea
[6]Proteomics Core Facility, Biomedical Research Institute, Seoul National University Hospital, Seoul 03080, Korea
[7]Graduate School of Life and Environmental Sciences, University of Tsukuba, Ibaraki 305-8577, Japan
[8]Ischemic/Hypoxic Disease Institute, Convergence Research Center for Dementia, Seoul National University College of Medicine, Seoul 03080, Korea
[9]These authors contributed equally
[10]Lead contact
*Correspondence: glickman@technion.ac.il (M.H.G.), minjlee@snu.ac.kr (M.J.L.)
https://doi.org/10.1016/j.celrep.2023.112701

SUMMARY

The 26S proteasome comprises 20S catalytic and 19S regulatory complexes. Approximately half of the proteasomes in cells exist as free 20S complexes; however, our mechanistic understanding of what determines the ratio of 26S to 20S species remains incomplete. Here, we show that glucose starvation uncouples 26S holoenzymes into 20S and 19S subcomplexes. Subcomplex affinity purification and quantitative mass spectrometry reveal that Ecm29 proteasome adaptor and scaffold (ECPAS) mediates this structural remodeling. The loss of ECPAS abrogates 26S dissociation, reducing degradation of 20S proteasome substrates, including puromycylated polypeptides. *In silico* modeling suggests that ECPAS conformational changes commence the disassembly process. ECPAS is also essential for endoplasmic reticulum stress response and cell survival during glucose starvation. *In vivo* xenograft model analysis reveals elevated 20S proteasome levels in glucose-deprived tumors. Our results demonstrate that the 20S-19S disassembly is a mechanism adapting global proteolysis to physiological needs and countering proteotoxic stress.

INTRODUCTION

The rate of proteolysis in a cell is a function of its physiological state, and the flux continuously changes in response to nutritional and environmental status. The ubiquitin (Ub)-proteasome system (UPS) is the primary cellular process responsible for degrading cytosolic, nuclear, and integral/peripheral membrane proteins under normal conditions. The UPS also controls protein quality by selectively proteolyzing misfolded and oxidatively damaged proteins.[1] Recent evidence suggests that aberrations in the UPS lead to the accumulation of potentially harmful proteins and, eventually, protein aggregates, a hallmark of aging and proteopathies.[2] If the proteasomal activity is compromised, *de novo* proteasome biogenesis is promoted, inducing a "bounce-back" response.[3] Unlike the UPS, autophagy usually operates at the basal level; however, during starvation or other types of stress, bulk autophagy is induced and indiscriminately breaks down cytoplasmic constituents to replenish anabolic intermediates.[4] The UPS and autophagy are also connected via intricate regulation mechanisms and coordinate their functions to maintain global proteolytic capacity.[5] As a result, identifying molecular etiologies contributing to abnormal proteostasis and developing pharmacological strategies modulating targeted or global proteolysis are active research areas.

The 26S proteasome is the primary ATP-dependent proteolytic holoenzyme in eukaryotes.[6] The conventional 26S proteasome consists of a catalytic 20S proteasome (hereafter referred to as 20S; molecular weight ~730 kDa) and either one or two loosely associated, but dissociable, 19S regulatory complexes (19S; ~930 kDa).[7] The doubly capped proteasome with a 19S-20S-19S configuration is also known as the 30S proteasome, distinguishing it from the singly capped 26S proteasome. Upon coming together in the 26S holoenzyme, the heptameric PSMA/α ring at the 20S surface and the hexameric AAA+ ATPase PMSC/Rpt ring at the base of the 19S form an asymmetric interface around a contiguous substrate translocation channel from the 19S base into the 20S lumen. The axial alignment between the 20S and 19S constantly fluctuates in response

to ATP hydrolysis, contributing to the proteolytic potency of 26S proteasomes. Although more than half of proteasomes exist in their free 20S form,[8] the 20S proteasome was regarded as a latent enzyme requiring activation. However, the physiological relevance of Ub-independent, 20S-mediated proteolysis in eukaryotes has been increasingly recognized, especially for degradation of disordered or oxidized proteins.[9] Furthermore, it was recently demonstrated that, when engaged with substrates, the 20S undergoes a considerable conformational change, including the "gate" opening.[10] In contrast to our advanced understanding of 26S proteasome assembly, substrate selection, and proteolytic processes, the exact mechanisms controlling the cellular levels of free 20S proteasomes as well as their contribution to cellular proteolysis remain largely elusive.

Large-scale changes in the proteome in response to environmental stressors require an enhanced proteolytic capacity of proteasomes to maintain protein quality and homeostasis. The inhibition of USP14/Ubp6 or phosphorylation of PSMD11/Rpn6 effectively increased proteasome activity and degradation of toxic proteins[11,12]; however, numerous endogenous substrates were insensitive to these activation methods. In response to severe stress conditions, 26S proteasomes are regulated in a spatiotemporal manner (instead of undergoing energy-costly degradation and synthesis) and packaged into membrane-less organelles, such as proteasome storage granules (PSGs; for example, during energy depletion), aggresomes (catalytic inhibition), or nuclear foci (hypertonic stress).[13–15] These proteasome inclusions are formed via reversible liquid-liquid phase separation (LLPS), allowing these condensates to re-dissipate into the nucleus or cytoplasm when the stress is removed.[16] This spatiotemporal regulation allows cells to rapidly adapt to proteostatic challenges, especially considering that the proteasome is a long-lived and abundant constituent of the cell.[17,18]

Nutrient deprivation triggers a transition of the cellular proteome from a proliferative state to a quiescent one. In yeast, in response to carbon depletion, cellular proteasomes are reversibly condensed into PSGs for protecting them from autophagic degradation.[19] In mammalian cells, however, the formation of PSGs is rarely reported and little is known about cellular proteasomal responses to metabolic challenges. In the current study, we discovered an unexpected adaptive response of 26S proteasomes to prolonged glucose depletion: the disassembly of 26S proteasomes into 20S and 19S subcomplexes. Using biochemical and proteomic approaches, we found that, during this conformational transition, the interaction between the 26S proteasome and a proteasome adaptor protein Ecm29 proteasome adaptor and scaffold (ECPAS)/Ecm29[20,21] was significantly shifted from the 20S to the 19S, triggering the disassembly. Consequently, deletion of *ECPAS* effectively abrogated the 20S-19S disassembly. Computational prediction analysis produced two distinct binding models of ECPAS to the assembled and disassembled states of proteasomes. We also demonstrated that free 20S generated under glucose-depleted conditions facilitated the degradation of misfolded proteins in a Ub-independent manner and prevented endoplasmic reticulum (ER) stress-induced cellular dysfunction and apoptosis. Finally, using a mouse xenograft model, we found that elevated levels of 20S proteasomes correlated with the reduced levels of glucose in tumor tissues. These findings suggest an essential pro-survival role for 26S proteasome disassembly that allows cells to cope with excess amounts of misfolded and potentially proteotoxic proteins in response to glucose-starvation conditions.

RESULTS

Dissociation of the 26S/30S proteasome into subcomplexes in response to glucose depletion

To elucidate the effect of different stress conditions on proteasomes, we tagged a 20S subunit PSMB2/β4 and a 19S subunit PSMD14/Rpn11 with tobacco etch virus (TEV) protease-cleavable hexahistidine-biotin (HB), which allowed a rapid affinity purification of human proteasomes using streptavidin beads (Figure 1A).[22] This method enabled the efficient isolation not only of proteasome holoenzymes (26S and 30S) but also of their subcomplexes (20S and 19S, respectively) from HEK293 cells stably expressing one of these tagged subunits. We observed that, in cells cultured in glucose-depleted medium for 12 h (final glucose concentration <0.2 mg/dL with serum supplementation, compared with regular media containing >450 mg/dL glucose), the population of purified PSMB2-HB proteasomes was markedly shifted from the 26S/30S composition to the 20S proteasome, using non-denaturing (native) electrophoresis and subsequent in-gel fluorogenic substrate (suc-LLVY-AMC) hydrolysis (Figure 1B). Silver staining and immunoblotting (IB) analysis following SDS-PAGE of proteasomes isolated using this tagged PSMB2-HB subunit showed that the protein levels of 19S base and lid components (PSMC2/Rpt1 and PSMD14, respectively) and 19S-interacting proteins, such as VCP/p97 and USP14/Ubp6, were significantly reduced during glucose starvation, while those of 20S proteasomes were comparable (Figure 1C). A similar compositional change in proteasomes was observed after affinity purification with different HB-tagged 20S subunits or from whole-cell lysates (WCLs) (Figures S1A–S1D). These results suggest that the disassembly of 26S proteasomes into the 20S and 19S is a prevalent response mechanism in glucose-starved mammalian cells.

We next performed parallel experiments using 19S-tagged PSMD14-HB proteasomes. This approach also showed a significant loss of interaction between the 20S and 19S after glucose deprivation (Figures 1D and 1E). The results were consistent with the previous observations using PSMB2-HB proteasomes except for a noticeable amount of 30S proteasomes from the glucose-deprived samples, which were formed by reassembling of the 26S and free 19S complexes in the eluted solution after TEV protease cleavage (Figure 1D). In both cases, the disassembled 20S and 19S subcomplexes appeared to retain their structural integrity (Figures 1B and 1D). To monitor the 26S disassembly in WCLs, the samples were gently fractionated by size-exclusion chromatography. Using subsequent native PAGE, we observed that, upon glucose depletion, a significant portion of 19S was disassembled from the 26S/30S species (Figure 1F). The glucose-starvation-mediated 26S disassembly occurred in a time-dependent manner over a 12-h time period (Figure S1E), possibly reflecting the gradual reduction of intracellular energy states. At the same time, the abundance of individual 26S proteasome subunits in WCLs and their mRNA levels were

CellPress
OPEN ACCESS

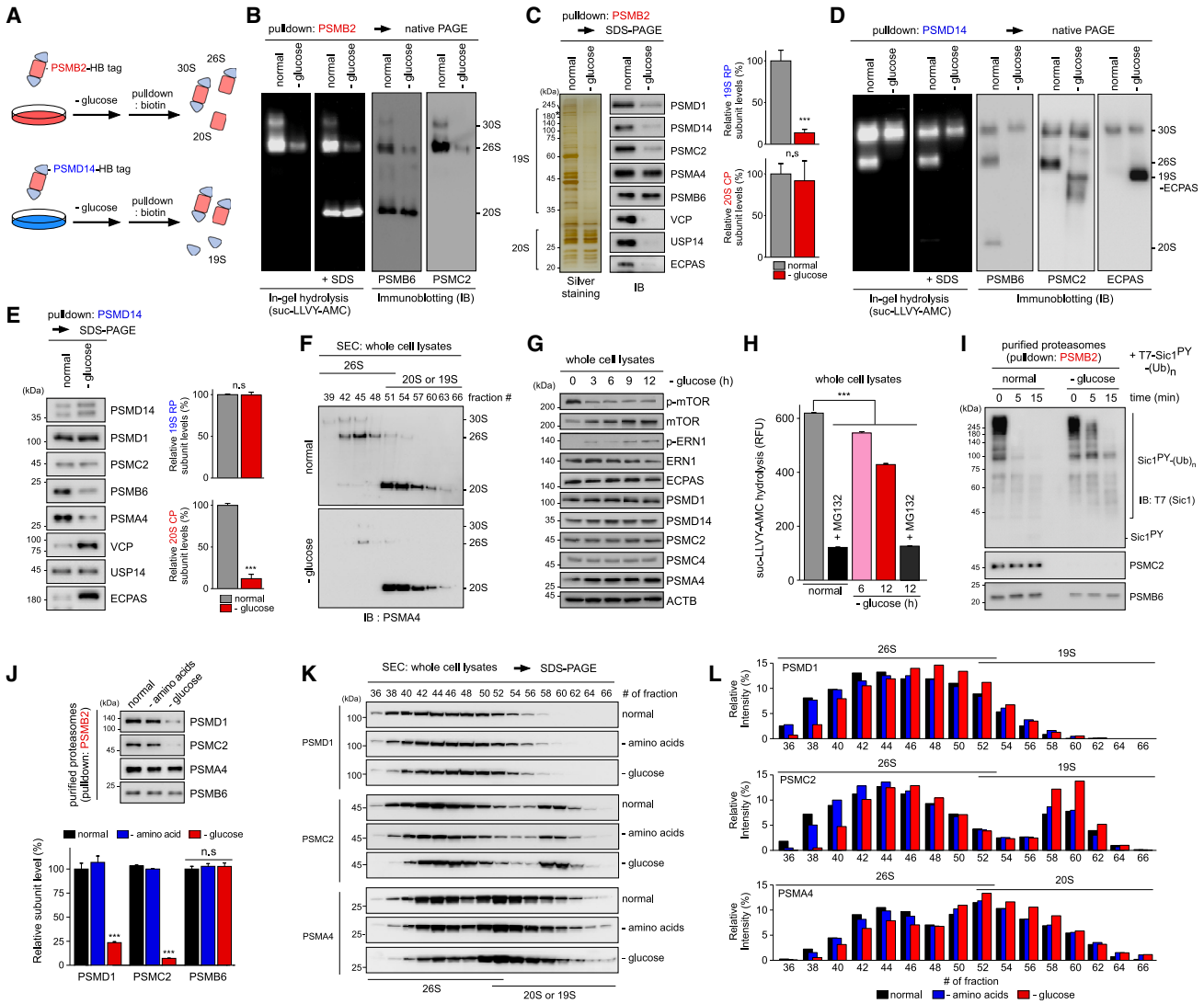

Figure 1. Glucose depletion leads to the disassociation of 20S and 19S subcomplexes

(A) Schematic representation of 26S proteasome-affinity tags and purification schemes used in this study. HEK293 cells stably expressing hexahistidine-biotin (HB)-tagged PSMB2/β4 or PSMD14/Rpn11 were treated with glucose-depleted media for subsequent proteasome affinity purification.

(B) Glucose depletion for 12 h triggered the dissociation of 26S proteasomes. Purified PSMB2-HB proteasomes were resolved by non-denaturing (native) polyacrylamide gel electrophoresis (PAGE), followed by visualization using in-gel suc-LLVY-AMC hydrolysis (left panels) and immunoblotting (IB; right panels). The addition of 0.02% SDS activated the 20S proteasome.

(C) As in (B), except that the proteasomes were analyzed using denaturing SDS-PAGE followed by silver staining and IB using various antibodies against the 20S and 19S subunits, and 19S-interacting proteins (left). Asterisk indicates ECPAS co-purified with proteasomes. Quantification of average 19S (PSMD1, PSMD14, and PSMC2) and 20S (PSMA4 and PSMB6) subunits signal (right). Each value was normalized to those average values of each 19S or 20S subunit's signal upon normal conditions. Values are represented as the mean ± SD of three independent experiments (N = 3); ***$p < 0.001$ (two-tailed Student's t test).

(D and E) 19S-tagged PSMD14-HB proteasomes were analyzed as in (B) and (C), respectively.

(F) Whole-cell lysates (WCLs) were analyzed using size-exclusion chromatography (SEC), and each fraction was subjected to native PAGE/IB.

(G) Time-dependent changes of the endogenous proteins in HEK293 cells during glucose depletion, analyzed by SDS-PAGE/IB.

(H) Proteasome activity was monitored through hydrolysis of the suc-LLVY-AMC using WCLs under normal and glucose-depleted conditions. A representative result from these independent experiments is shown. Each bar represents the mean (±SD) of three independent experiments (N = 3); ***$p < 0.001$ (one-way ANOVA followed by Bonferroni's *post hoc* test).

(I) Polyubiquitinated Sic1 ($Sic1^{PY}$-Ub_n) protein was incubated with purified PSMB2-HB proteasomes, and its degradation was examined using SDS-PAGE/IB.

(J) The subunits of purified proteasomes were compared after depriving of amino acids or glucose from the media for 12 h using SDS-PAGE/IB (upper). For quantification, signals from PSMD1, PSMC2, and PSMB6 were normalized to those of PSMA4 (lower). Bars represent the mean ± SD of three independent experiments (N = 3); ***$p < 0.001$ (one-way ANOVA followed by Bonferroni's *post hoc* test); n.s., not significant.

(K) SEC analysis after 12 h of depletion of amino acids or glucose was performed and each fraction was subjected to SDS-PAGE/IB for proteasome subunits.

(L) Quantitation of (K). Percentage of proteasome subunit signals from each fraction were measured and plotted. See also Figure S1.

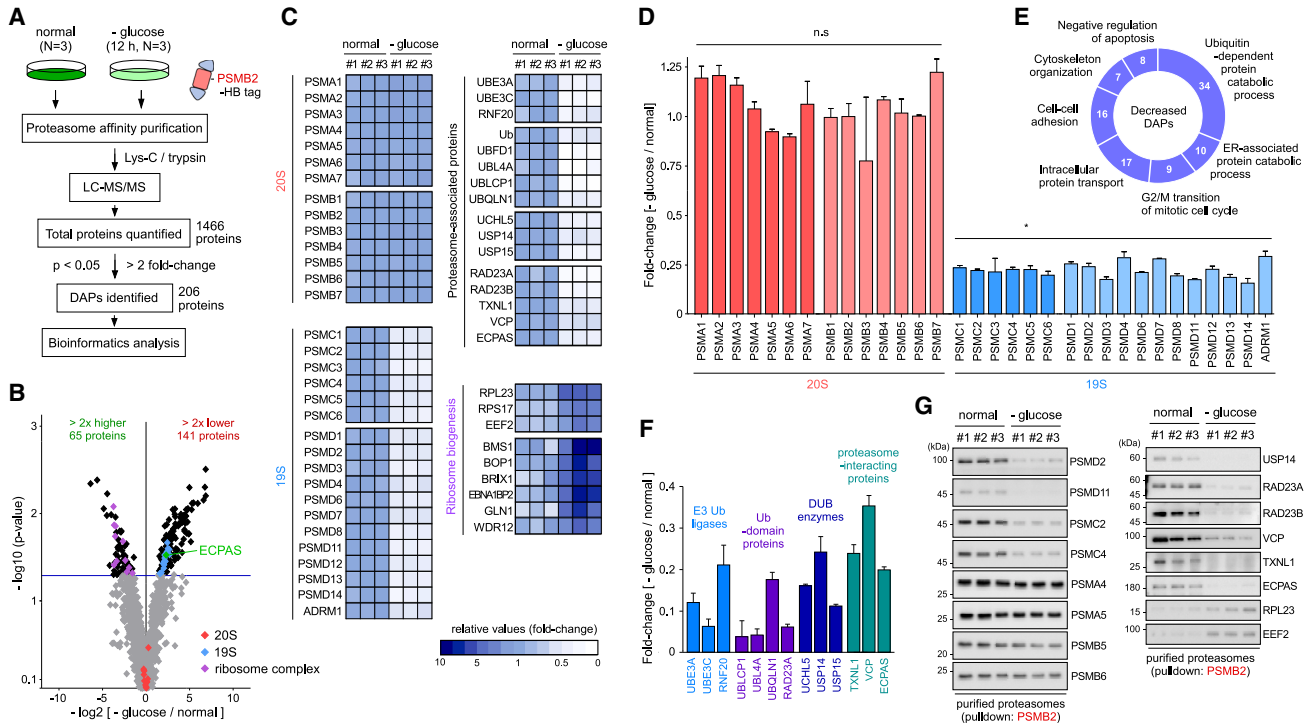

Figure 2. Analysis of proteasome disassembly using quantitative MS

(A) Overview of quantitative MS analysis with the label-free, intensity-based absolute quantification (iBAQ) method, using affinity-purified PSMB2-HB proteasomes. A total of 206 differentially associated proteins (DAPs) were identified in the PSMB2-HB proteasomes after 12 h of glucose depletion.

(B) Volcano plot of the total identified proteins. The blue line shows the threshold of p value ($p < 0.05$). Non-DAPs are shown in gray ($p > 0.05$ or <2-fold change in log2 ratios of glucose starvation to normal conditions). Red, blue, and purple dots depict unchanged 20S subunits, downregulated 19S subunits, and upregulated ribosome complex subunits, respectively.

(C) The heatmap shows distinct changes in the relative abundance of proteasome subunits, proteasome-associated proteins, and ribosome biogenesis-related proteins. Degrees of upregulation (darker blue) and downregulation (lighter blue to white) are explained in the color key.

(D) Relative abundance changes of the constitutional subunits of 26S proteasomes. Data represented include the mean ± SD of three independent experiments (N = 3); *$p < 0.05$ (one-way ANOVA with Bonferroni's multiple comparison test); n.s., not significant.

(E) Classification of downregulated DAPs into different biological pathways using Gene Ontology analysis. Of the 141 DAPs, 34 proteins were enriched in Ub-dependent proteolysis, 17 in intracellular protein transport, and 10 in ER-associated proteolysis.

(F) Representative decrease in the quantity of proteasome-associated proteins, including E3 ubiquitin (Ub) ligases and deubiquitinating (DUB) enzymes, following glucose depletion.

(G) Validation of DAPs using IB analysis against the 20S, 19S, and proteasome-associated proteins in normal and glucose-depleted conditions. See also Figure S2.

not affected during the starvation period (Figures 1G and S1F). We also observed a rapid decrease in mammalian target of rapamycin (mTOR) phosphorylation (starting at ~3 h post glucose depletion) and a gradual increase in ER to nucleus signaling 1 (ERN1/IRE1) phosphorylation (peaking at ~9 h) (Figure 1G), corresponding to the inhibition of the mTOR signaling pathway and activation of unfolded protein responses (UPRs), respectively. Proteasomes in the starved cells were largely dispersed throughout the cells without forming noticeable foci such as PSGs (Figures S1G and S1H). Upon re-incubation of starved cells with a glucose-containing medium, the isolated PSMB2-HB and PSMB5-HB proteasomes from HEK293 and A549 cells, respectively, were retrieved as the 26S form (Figure S1I), indicating that this conformational change is a reversible process influenced by the intracellular glucose concentration.

Next, we evaluated the total activity of proteasomes in WCLs using suc-LLVY-AMC, a substrate considered to be more specific toward the chymotrypsin-like PSMB5 activity but generally accepted to represent overall proteasome activity. We observed that total cellular proteasome activity progressively decreased with glucose deprivation (Figure 1H). Generally, the specific peptidase activity of the 20S is lower than that of the 26S proteasome,[10] consistent with a transition from 26S to 20S species during glucose deprivation. Furthermore, the purified PSMB2-HB proteasomes also showed considerably lower peptidyl substrate hydrolytic activity in response to glucose deprivation (Figure S1J). When we incubated these purified proteasomes with polyubiquitinated Sic1 containing PY motif (Ub-Sic1^{PY}), which is a more physiological substrate than fluorogenic peptides,[23] the degradation of Ub-Sic1^{PY} was significantly delayed in the PSMB2-HB proteasomes purified during glucose starvation compared with that in control proteasomes (Figures 1I, S1K, and S1L). We note that the 26S proteasome disassembly was not observed in response to amino acid or serum deprivation

during the same time points (Figures 1J–1L and S2A) and mTOR inhibition or AMP-activated kinase (AMPK) activation (Figures S2B and S2C). Therefore, our data indicate that the mechanism underlying the glucose-sensitive 26S proteasome assembly/disassembly is different from the cellular adaptation responding to AMPK activation or mTOR inhibition.

Identification and quantification of changes in proteasome composition and interacting proteins during glucose depletion

To explore the molecular mechanism underlying 26S/30S proteasome disassembly during glucose depletion, we performed a mass spectrometry (MS) analysis with an intensity-based absolute quantification (iBAQ) algorithm, which allows precise protein quantification without labeling. HEK293-PSMB2-HB stable cells were cultured under normal and glucose-starvation conditions for 12 h, and proteasomes and their interacting proteins were purified using streptavidin pull-downs for the iBAQ-MS analysis (Figure 2A). Using our cutoff criteria (threshold at 2-fold change in absolute quantity and adjusted p value <0.05; see STAR Methods for details), we identified a total of 206 differentially associated proteins (DAPs). Among them, 141 proteins had significantly reduced binding affinity toward PSMB2-HB proteasomes, while 65 had increased affinity after 12 h of glucose deprivation (Figure 2B; Table S1). Our quantitative DAP profile indicated that, under glucose-depleted conditions, the levels of constituent 19S subunits were markedly decreased to ~20% of the normal levels (Figures 2C and 2D), substantiating our biochemical findings (Figure 1). The levels of proteasome activators (PSME1–4), were unchanged (Table S2), suggesting that hybrid proteasomes such as the 11S-20S complex are not significantly involved in proteasome dynamics during glucose depletion, although the potential alternative capping on the proteasome remains to be further evaluated.

Gene Ontology analysis revealed that DAPs with decreased affinity were clustered within several biological processes, such as Ub-dependent protein catabolism, ER-associated protein catabolism, intracellular protein transport, and negative regulation of apoptosis (Figure 2E). As expected, in response to stress, the majority of 19S-interacting proteins were also lost from affinity-isolated proteasome complexes, including E3 Ub ligases (UBE3A, UBE3C, and RNF20), Ub and Ub-domain proteins (RAD23A, UBFD1, UBL4A, UBLCP1, and UBQLN2), deubiquitinating enzymes (UCHL5, USP14, and USP15), and other known proteasome-associated proteins (TXNL1, VCP, and ECPAS) (Figure 2F and Table S3). In sharp contrast, another set of DAPs had increased association with PSMB2-HB proteasomes in response to glucose starvation (Figures 2B and 2C). Notably, we found that many RNA-binding and ribosomal proteins associated directly with the 20S proteasome were significantly higher in the glucose-depleted group than in the control groups (Figures 2B, 2C, and S2D–S2G; Table S3). These findings suggested that, under stress conditions, proteasome disassembly may affect not only the degradation of existing proteins but also *de novo* protein synthesis, reshaping the global proteome. Next, we performed IB to validate our proteomics data, using PSMB2-HB proteasome, and found that the level changes in co-purified proteins, such as downregulated RAD23 A/B, VCP, and ECPAS, and upregulated RPL23 and EEF2, were consistent with the results of iBAQ-MS analysis (Figures 2G and S2G). Taken together, our label-free quantitative MS analysis demonstrated that, in response to glucose depletion, the 26S proteasome holoenzyme effectively dissociates into the 20S and 19S, together with a significant interactome change in numerous proteasome-associated proteins.

ECPAS-dependent regulation of human 26S/30S proteasomes upon glucose depletion

One possible explanation for 26S proteasome dissociation under glucose-depleted conditions could be insufficient ATP hydrolysis by the PSMC AAA+ ATPase ring, which is required for strengthening the 20S-19S interaction. However, we observed that, even after glucose starvation for 12 h, cellular ATP levels decreased only to ~70%–80% of control levels (Figure S3A). Furthermore, the treatment of cells with proteasome inhibitors known to stabilize the interaction between the 20S and 19S without requiring ATP hydrolysis[24] potently delayed proteasome disassembly (Figures S3B and S3C). These results suggested that the observed proteasome remodeling was mediated by a regulated process rather than ATP deficiency. Based on our proteomics data (Figures 2B, 2C, and 2F), we postulated that the proteasome adaptor protein ECPAS may play a role in 26S disassembly. Ecm29, the yeast homolog of ECPAS, was initially identified as a salt-sensitive proteasome component that stabilizes the 26S/30S proteasomes in yeast.[20] However, in mammalian cells, ECPAS was reported to induce the dissociation of the holoenzymes in response to oxidative stress,[25] although its physiological function remains largely obscure.

Our purification system showed that ECPAS was co-purified with both PSMB2-HB and PSMD14-HB proteasomes under normal conditions, while it was bound only to PSMD14-HB complexes but not to PSMB2-HB under glucose-depleted conditions (Figures 1C–1E, and 3A). Native PAGE analysis showed that ECPAS co-migrated with 19S complexes under glucose-depleted conditions (Figure 1D), further demonstrating that ECPAS-proteasome binding shifted from the 26S to the 19S, depending on glucose availability. To estimate the stoichiometric abundance of ECPAS compared with the proteasome, we performed the MS-iBAQ analysis using the separated 20S, 26S, and 30S proteasomes on native gel electrophoresis. The abundance of ECPAS to the proteasome in each complex was determined by calculating the ratio between the iBAQ value of ECPAS and the average iBAQ value of all 20S proteasome subunits (PSMA1–7 and PSMB1–7). The relative amount of ECPAS was ~4.9% of the 26S and ~11.5% of the 30S (Figure S3D; Table S4). These values are in accordance with the quantifications from mass photometry-based analysis[26] and the molar ratio of 19S between the singly capped 26S and doubly capped 30S proteasomes, defining ECPAS as a sub-stoichiometric 19S-interacting protein.

The results presented above indicated that ECPAS was potentially involved in 20S-19S disassembly; therefore, to confirm these findings, we examined the consequences of overexpressed ECPAS under normal conditions on 26S disassembly, but it had little effect on the 20S-19S disassembly (Figure S3E). We also investigated the role of ECPAS using loss-of-function experiments. The knockdown and knockout of *ECPAS* in

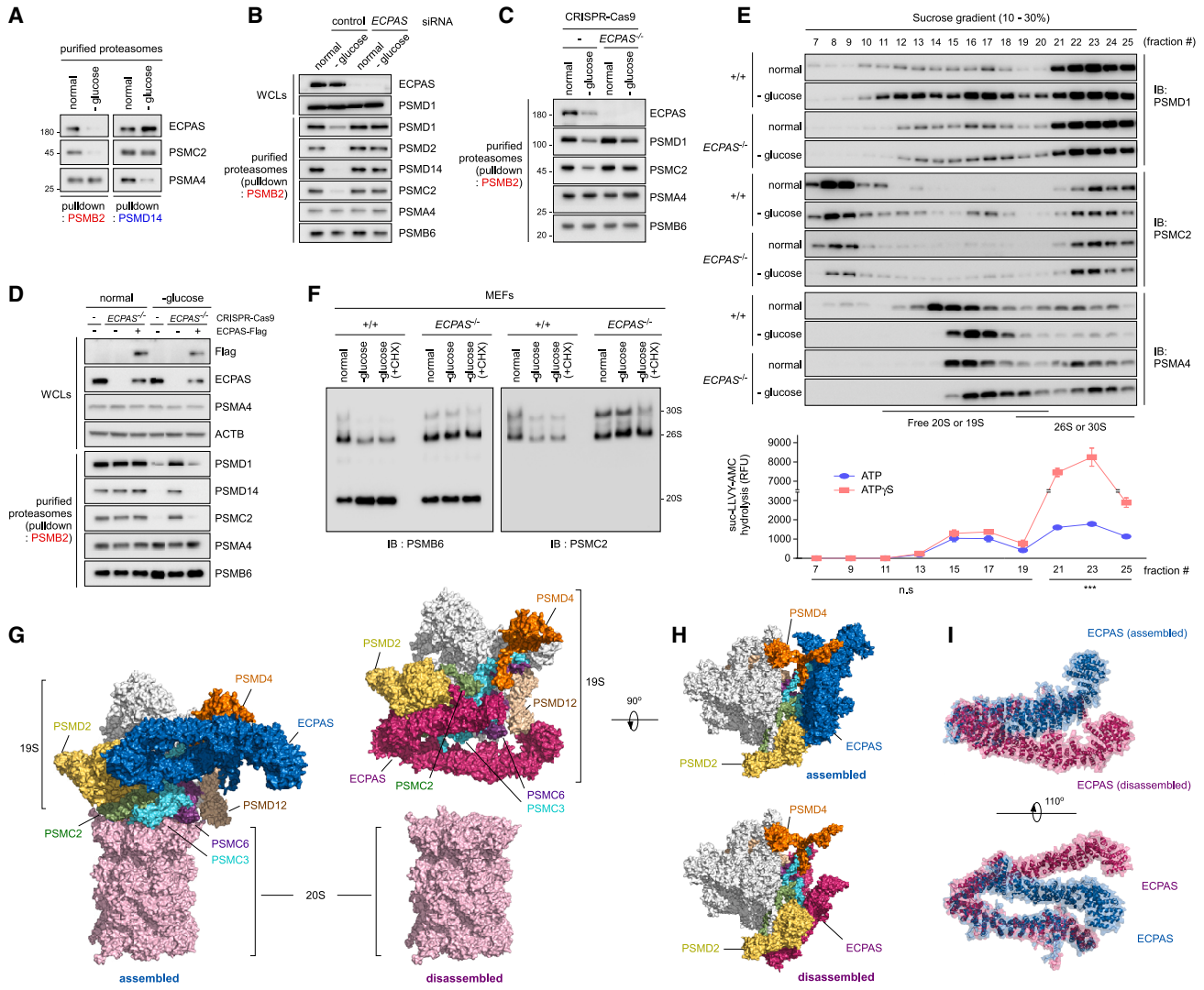

Figure 3. ECPAS/Ecm29 mediates 26S/30S proteasome disassembly in response to glucose depletion

(A) Direct interactions between endogenous ECPAS and purified PSMB2-HB (left) or PSMD14 (right) proteasomes under normal conditions are shown. Cellular proteasomes were pulled down using streptavidin beads under normal and 12-h glucose-depleted conditions and analyzed by SDS-PAGE/IB using anti-ECPAS antibodies. Glucose depletion induced a strong dissociation of ECPAS from the 20S proteasomes but resulted in a tighter binding to the 19S complex than did normal conditions.

(B) HEK293-PSMB2-HB cells were transfected with scrambled (control) or *ECPAS* siRNA for 48 h and then cultured in glucose-deprived medium for an additional 12 h. Purified PSMB2-HB proteasomes were subjected to SDS-PAGE/IB using indicated antibodies.

(C) As in (B), except that the experiments were conducted with *ECPAS* knockout (HEK293-PSMB2-HB$^{ECPAS-/-}$) cells generated by the CRISPR-Cas9 system.

(D) Adding back ECPAS to the knockout cells. HEK293-PSMB2-HB$^{ECPAS-/-}$ cells were transfected with ECPAS-expressing plasmids for 36 h and then incubated in glucose-depleted medium for 12 h. PSMB2-HB proteasomes were affinity purified, separated using SDS-PAGE, and then probed with antibodies against the 20S or 19S subunits.

(E) Sucrose-gradient ultracentrifugation of WCLs from wild-type and *ECPAS*$^{-/-}$ mouse embryonic fibroblasts (MEFs) grown in standard or glucose-depleted medium for 12 h. Fractionated samples were analyzed by SDS-PAGE/IB (upper). The fractions containing 26S/30S proteasomes showed significantly elevated (~8-fold) suc-LLVY-AMC hydrolysis in the presence of ATPγS (lower).

(F) Wild-type (+/+) and *ECPAS*$^{-/-}$ MEFs were cultured for 12 h under normal and glucose-depletion conditions supplemented with DMSO or 80 μg/mL cycloheximide (CHX). WCLs were analyzed using native PAGE/IB.

(G and H) Modeled conformations of ECPAS-26S proteasome complex predicted by AlphaFold and GalaxyTongDock (an *ab initio* docking algorithm), viewed from the side (G) and top (H). Two distinct conformations were generated and designated as the assembled and disassembled states, in the latter of which ECPAS sterically obstructs the 19S-20S interface.

(I) Structural comparison of the ECPAS structures in the assembled and disassembled states (shown in cobalt and magenta, respectively). The modeled structures are superimposed with the coincided N-terminal portions and are shown from different perspectives. See also Figures S3 and S4.

CellPress
OPEN ACCESS

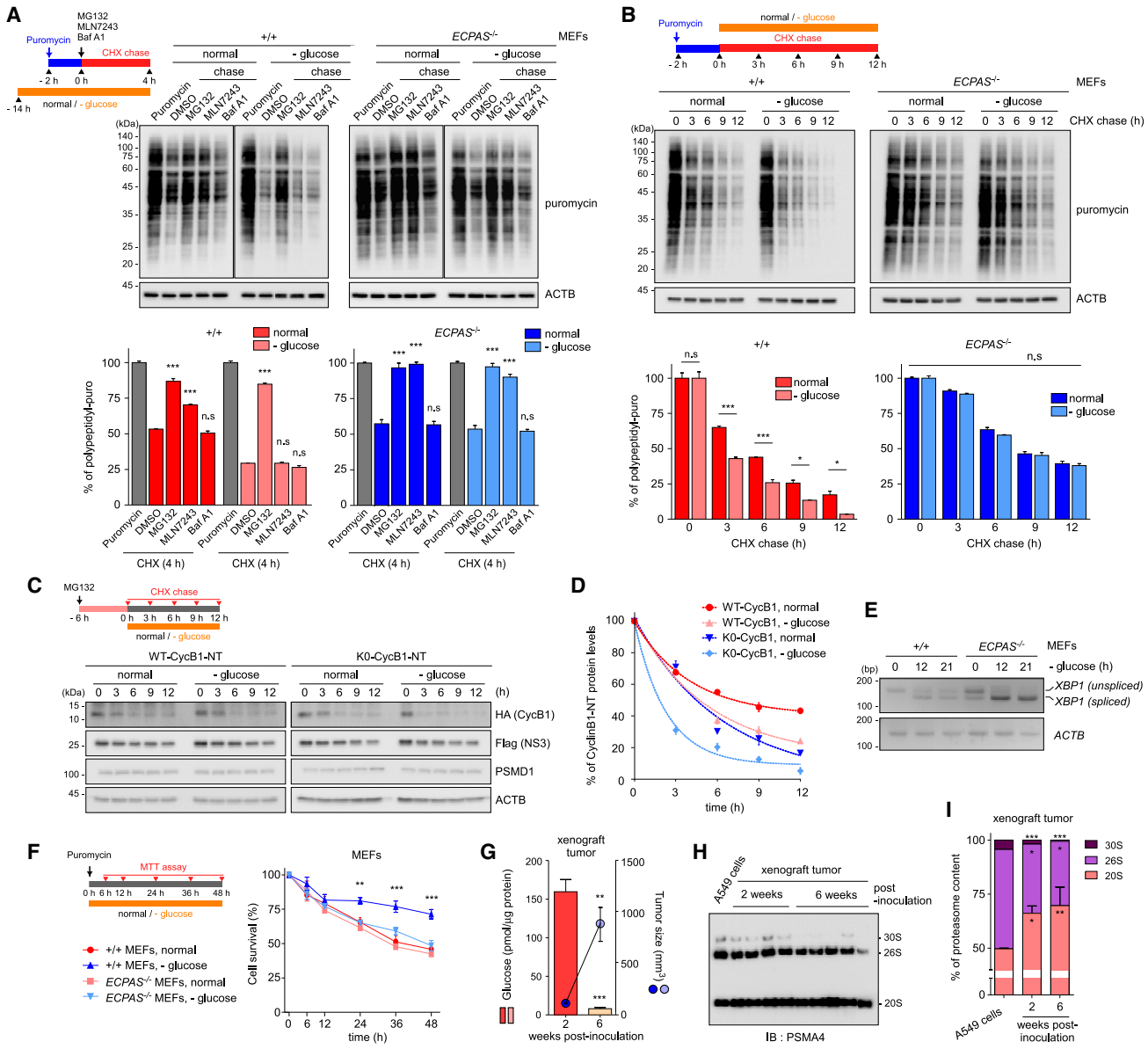

Figure 4. Free 20S proteasomes facilitate Ub-independent substrate degradation and contribute to cell survival under glucose depletion

(A) Wild-type (+/+) and *ECPAS*$^{-/-}$ MEFs were cultured for 12 h under normal and glucose-depletion conditions, followed by a 2-h puromycin (5 μg/mL) treatment and a subsequent 4-h cycloheximide (CHX; 80 μg/mL) chase experiment. The CHX chase was performed in the presence of DMSO, the proteasome inhibitor MG1312 (10 μM), the E1 Ub-activating enzyme inhibitor MLN7243 (1 μM), or the autophagic flux inhibitor bafilomycin A1 (BafA1; 100 nM). SDS-PAGE/IB for puromycylated polypeptides (upper); their quantities were normalized to those of endogenous ACTB/β-actin (lower). Shown are the average percentages of remaining polypeptidyl-puro (mean ± SD) from three independent experiments (N = 3); ***p < 0.001 (one-way ANOVA followed by the Bonferroni *post hoc* test).

(B) As in (A), except that the chase experiment was performed for the various time periods. *p < 0.05, ***p < 0.001 (one-way ANOVA followed by the Bonferroni *post hoc* test; N = 3).

(C) HEK293 cells were transfected with the wild-type and lysine-less mutant of cyclin B1 N-terminal segment (WT-CycB1-NT and K0-CycB1-NT, respectively) for 24 h, cultured in normal and glucose-depleted medium for indicated periods, and prepared for IB analysis to examine CycB1-NT degradation.

(D) Quantification of HA-CycB1-NT signals in (C) normalized to those of co-expressed flag-NS3.

(E) mRNA levels of unspliced and spliced *XBP1* in +/+ and *ECPAS*$^{-/-}$ MEFs after glucose starvation (12 h). Semi-quantitative RT-PCR (25 cycles) and quantitative normalization were performed using ACTB gene expression.

(F) Cell survival upon puromycin exposure and glucose starvation. Cells were cultured in normal or glucose-depleted medium in the absence or presence of puromycin (250 ng/mL) for up to 48 h, and their survival was quantified using an MTT assay. **p < 0.01, ***p < 0.001 (one-way ANOVA followed by the Bonferroni *post hoc* test; N = 3).

(G) Glucose was significantly depleted in late-stage tumors derived from mouse xenograft models. A549 cells (5 × 10^5) in 0.1 mL of PBS/Matrigel were subcutaneously injected into the dorsa of nonobese diabetic (NOD)/severe combined immunodeficiency (SCID) mice at the right-hind flank. Tumor tissues were

(legend continued on next page)

HEK293-PSMB2-HB cells using small interfering RNA (siRNA) and the CRISPR-Cas9 system, respectively, stabilized PSMB2-isolated 26S/30S proteasomes even under glucose-depleted conditions (Figures 3B and 3C) and 20S-19S assembly/disassembly was not affected by *TXNL1* or *VCP* knockdown (Figure S3F). To further verify the involvement of ECPAS in 26S proteasome remodeling, HEK293-PSMB2-HB$^{ECPAS-/-}$ cells were transfected with ECPAS, which rescued the biochemical phenotype of 26S proteasomes during glucose starvation (Figure 3D).

The association/dissociation between the 20S and 19S subcomplexes was also analyzed in WCLs from wild-type (+/+) and *ECPAS*$^{-/-}$ mouse embryonic fibroblasts (MEFs) using sucrose-gradient ultracentrifugation. In contrast to +/+ MEFs, glucose starvation in *ECPAS*$^{-/-}$ MEFs did not significantly change the levels of proteasome subunits in the earlier fractions containing free 20S or 19S complex (Figure 3E). The fractionated samples were further analyzed using native PAGE; the results showed that, after glucose deprivation, the proportion of 26S/30S proteasomes in *ECPAS*$^{-/-}$ MEFs was significantly increased compared with that in +/+ MEFs (Figure S4A). Native PAGE with subsequent IB analysis also revealed that changes in the 20S-19S interaction were independent with cycloheximide (Figures 3F and S4B). In addition, we found that, following carbon source starvation or during the stationary phase, yeast proteasomes in an Ecm29Δ strain consistently had a higher ratio of 26S/30S configuration to free 20S than did those from the control strain (Figure S4C). The phenotypic similarity between yeast and mammalian proteasomes suggests that the 26S proteasome dissociation mediated by ECPAS/Ecm29 is evolutionarily conserved in eukaryotes, possibly as a global protein quality control mechanism during glucose starvation.

Conformational switch of ECPAS to induce 19S-20S disassembly

To gain mechanistic insight into the ECPAS-mediated disassembly of 26S proteasomes, we performed *in silico* modeling to determine the structure of the ECPAS-26S proteasome complex. The free ECPAS structure (UniProt: Q5VYK3) was predicted by AlphaFold to have a horseshoe-shaped fold with a high confidence score (median pLDDT = 88.4 from residues 1 to 1,845) (Figure S4D). The overall morphology was similar to yeast Ecm29 structures obtained by the Finley group using electron microscopy ~20 years ago.[20] The AlphaFold-predicted structures of yeast Ecm29 and human ECPAS were highly analogous, even though the amino acid identity between them is only 25.5%. The two segments showing high sequence similarity between yeast Ecm29 and human ECPAS, were located in the two stretched branches with many HEAT repeats. On the contrary, the angled region between them, located at the residues 1,048–1,148, had low confidence scores (median pLDDT = 65.89). To predict the interaction between ECPAS and the 26S proteasomes (PDB: 6MSB), we employed an *ab initio* protein-protein docking algorithm termed GalaxyTongDock (see STAR Methods for details) and obtained two distinct complex models (Figures 3G and 3H), which may represent the "assembled" and "disassembled" conformations between the 20S and 19S subcomplexes.

In the assembled states, the N-terminal shank of ECPAS directly interacted with the proteasome-residing Ub receptors, such as PSMD2/Rpn1 and PSMD4/Rpn10, on the face of the 19S (Figures 3G and 3H). The Ub-interacting motifs of PSMD2 and PSMD4 were excluded from the ECPAS-19S interaction, ruling out the potential inhibitory effect of ECPAS binding on normal proteasome functions. In the disassembled state, the horseshoe curvature at the low-pLDDT region of ECPAS was noticeably altered, while the overall conformational landscape of ECPAS was only slightly changed (Figure 3I). Simultaneously, the C-terminal region of ECPAS in this conformation protruded toward the hexameric PSMC ring/heptameric PSMA ring interface, potentially obstructing their association. Therefore, the conformational change of ECPAS might be the primary regulatory checkpoint for the disassembly of the 26S upon glucose starvation. These results imply that our integrative *in silico* modeling algorithm with a predictive power of AlphaFold can predict a highly plausible biochemical mechanism (e.g., the dissociative role of ECPAS in the 20S and 19S), complementing conventional approaches. However, how ECPAS structures are changed and what signaling pathways regulate this process remain to be elucidated.

Facilitated degradation of misfolded proteins by 20S proteasomes during glucose depletion

The 20S proteasome proteolyzes fully or partially disordered substrates in a Ub- and ATP-independent manner. To investigate the contribution of disassembled 20S proteasomes under glucose-starvation conditions to the removal of misfolded proteins, we first used puromycin, which incorporates nascent polypeptides into their C termini, generating inherently disordered puromycylated polypeptides. In +/+ MEFs and A549 cells, we observed that puromycylated polypeptides were degraded more rapidly in glucose-depleted media than in control media (Figures 4A, 4B, S5A, and S5B). This preferential removal of the polypeptidyl-puro species was effectively abrogated by treatment with the proteasome inhibitor MG132 but was virtually unaffected by other inhibitors, such as bafilomycin A1 (autophagy/lysosomal inhibitor) or MLN7243 (E1 Ub-activating enzyme inhibitor) (Figures 4A and S5A). Independently, we observed the induction of autophagy-related factors during glucose starvation (Figures S1F and S5D); however, bafilomycin A1 treatment had little effect on the degradation of polypeptidyl-puro species (Figures 4A and S5A). These results indicated that lysosomal targeting or Ub modification is not the major clearance route for nascent misfolded proteins at least during glucose-deficient stress. In contrast to the results above, the steady-state levels of puromycylated polypeptides in *ECPAS*$^{-/-}$ MEFs were

harvested 2 and 6 weeks post inoculation (N = 4 and 5, respectively). Glucose levels normalized to the total protein concentration were compared with tumor sizes. Data are presented as the mean ± SEM; $^{**}p < 0.01$ and $^{***}p < 0.001$ (unpaired Student's t test).

(H) Elevated levels of the 20S proteasomes under more glucose-depleted conditions. Whole tumor tissue extracts with different xenograft periods were subjected to native PAGE followed by IB against PSMA4. WCLs from cultured A549 cells were used as controls.

(I) The relative amounts of the 20S, 26S, and 30S proteasomes were quantified from (H). Data are presented as the mean ± SD; $^{*}p < 0.05$, $^{**}p < 0.01$, and $^{***}p < 0.001$ (one-way ANOVA followed by the Bonferroni *post hoc* test). See also Figure S5.

largely comparable between normal and glucose-depleted conditions. At the same time, their levels in the knockout cells substantially increased in response to MG132 and MLN7243, but not bafilomycin A1 treatment (Figure 4A). These observations are in line with a role of free 20S in the removal of misfolded proteins under stress conditions. Cycloheximide chase experiments, conducted after a 2-h puromycin labeling, also showed that the degradation of puromycylated polypeptides in *ECPAS*$^{-/-}$ MEFs was significantly delayed, probably due to the impaired 20S-19S disassembly (Figure 4B). These results indicate that free 20S proteasomes play a key role in the clearance of nascent misfolded proteins under glucose-deficient conditions.

Since both 26S and 20S proteasomes have common catalytic sites and mechanisms, the remaining 26S may affect the degradation of polypeptidyl-puro species. To confirm the contribution of 26S proteasome disassembly to Ub-independent proteolysis, we utilized lysine-less mutants (K0) of the intrinsically disordered N-terminal segment of cyclin B1 (CycB1-NT), which is shorter lived than full-length CycB1 and directly proteolyzed by 20S proteasomes.[10] Transiently overexpressed K0-CycB1-NT was more rapidly turned over than wild-type counterparts (WT-CycB1-NT), while co-expressed NS3 levels were essentially unchanged (Figure 4C). Similar to the polypeptidyl-puro species, K0-CycB1-NT degradation was significantly accelerated under glucose-depleted conditions (half-lives 5.2 h vs. 2.4 h), while WT-CycB1-NT half-lives were modestly decreased (half-lives 8.7 h vs. 5.9 h; Figures 4C and 4D). mRNA levels of K0-CycB1-NT were little changed during glucose starvation (Figure S5C), indicating that the reduction of this model 20S substrate was indeed post-translational. Collectively, these data strongly indicate that disassembled 20S proteasomes were more efficient at proteolyzing disordered proteins in a Ub-independent manner than 26S proteasomes. This property is expected to be a cell survival strategy in response to glucose starvation that restrains cellular protein folding capacity and produces more misfolded and unstructured proteins.

We further investigated whether the rapid removal of misfolded proteins by the 20S proteasome is advantageous for maintaining proteostasis and subsequently cell survival. Previous studies demonstrated that glucose depletion induced ER stress and the UPR.[27] We observed that our stress condition (glucose deprivation for 12 h) also strongly increased the levels of ER stress markers and UPR signaling (Figures S5D and S5E). To evaluate the role of disassembled 20S proteasome in response to ER stress, we examined the ERN1-mediated splicing of X-box binding protein 1 (*XBP1*) mRNA, an evolutionarily conserved transcription factor required for the activation of the UPR.[28] RT-PCR analysis showed that glucose-starved *ECPAS*$^{-/-}$ MEFs produced significantly more spliced *XBP1* mRNA than +/+ MEFs (Figure 4E). Additional quantitative RT-PCR analysis revealed the upregulation of numerous genes involved in the ATF4-CHOP axis in response to glucose depletion (Figure S5F). Notably, the levels of these genes, which are involved in UPR-mediated apoptosis, were significantly higher in *ECPAS*$^{-/-}$ MEF than in +/+ MEFs (Figure S5F), indicating that the loss of *ECPAS* resulted in hypersensitivity to glucose-depletion-mediated ER stress. When puromycylated polypeptides were overexpressed, we found that *ECPAS*$^{-/-}$ MEFs had significantly higher cytotoxicity than did +/+ MEFs after prolonged glucose deprivation (Figure 4F). These results collectively indicate that proteasome disassembly upon glucose depletion is an effective compensatory strategy to degrade structurally disordered proteins and to provide a survival benefit to cells under ER stress.

Tumorigenesis is a pathological condition characterized by energy depletion, and, in human tumor tissues, it is known that glucose levels are significantly lower than those in normal tissues.[29] When we examined mouse tumor tissues from various xenograft models in different stages, we found that glucose concentrations were more drastically reduced in late-stage tumors than in early-stage tumors (159.6 ± 54.6 pmol/μg glucose concentration and 111.9 ± 5.6 mm^3 tumor volume in 2-week post-inoculation samples vs. 8.1 ± 5.8 pmol/μg and 877.8 ± 368.9 mm^3 in 6-week samples; Figure 4G). In addition, the 20S proteasome/total proteasome ratios were significantly higher in tumors (66.1% ± 3.4% and 69.7% ± 8.6% in 2- and 6-week samples, respectively) than in parental A549 cells (49.7% ± 0.3%) and they were negatively correlated with the glucose concentration (Figures 4H and 4I). These data indicate that the 26S proteasome disassembly may confer glucose-deficient cells with the ability to degrade various substrates in a Ub-independent manner during tumorigenesis and, therefore, present alternative therapeutic strategies for cancer. Tumor suppressor proteins such as p53 and retinoblastoma are known to be degraded in this manner, increasing cell death resistance and cell-cycle arrest.[30] Depletion of 26S or 30S holoenzymes accompanied by a concomitant increase in free 20S proteasomes may be a mechanism to shift cellular metabolism to a less regulated but more essential form of intracellular proteolysis, potentially serving as a hallmark of cancer.

DISCUSSION

Intracellular proteolytic mechanisms have evolved to allow cell survival in unfavorable environments. To maintain protein quality control, as well as the cellular amino acid pool, it is essential to promptly adjust the overall output of cellular proteolysis in response to the excess amounts of to-be-degraded substrates. Here, we report that the 26S and 30S proteasomes are dissociated into the 20S and 19S subcomplexes during glucose deprivation and are reversibly re-associated when the stress is relieved (Figure 5). During the stress, proteolytic activities attributed to 20S proteasomes increased, suggesting that 26S disassembly is not necessarily a mechanism to attenuate proteolysis but rather to alter substrate specificity. ECPAS showed increased affinity toward the 19S in the disassembly process and its deletion resulted in a delayed 26S disassembly process in mammals. Moreover, as a mechanistically similar process was observed in budding yeast—which is more sensitive to variations in glucose availability and even more tolerant to drastic reduction in its metabolic activity upon extreme starvation—the disassembly of 26S proteasome under glucose-starved conditions transpired to be an evolutionarily conserved mechanism necessary for global proteostasis and cell survival. Our *in silico* analysis implies that conformational rearrangement of ECPAS may function as a necessary process for disengaging PSMC hexameric ring from the PSMA heptameric ring. As an underlying mechanism, it seems plausible that post-translational modifications (PTMs) of ECPAS generated during

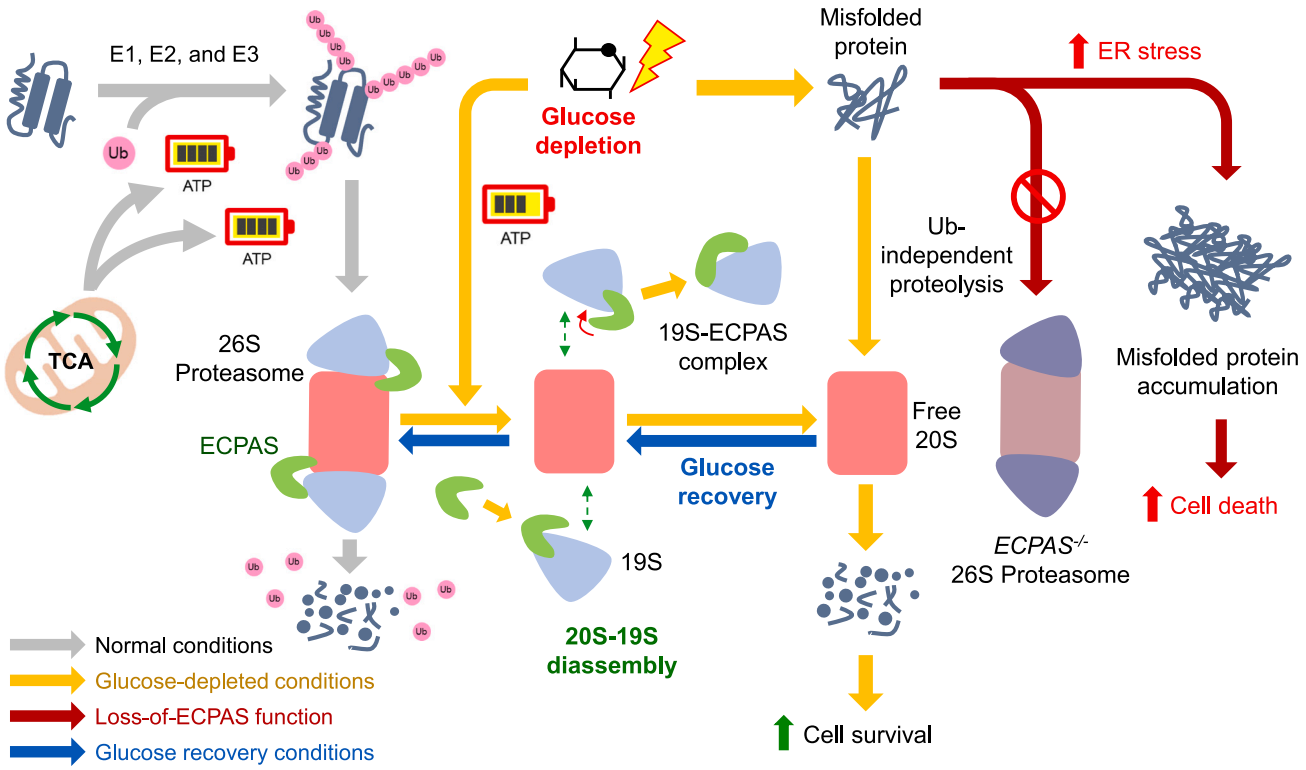

Figure 5. A model of proteasome disassembly upon glucose starvation as an adaptive survival strategy

Under normal conditions, the 26S-30S proteasome degrades polyubiquitinated protein in a Ub- and ATP-dependent manner. When a cell experiences low levels of available glucose, the 26S-30S proteasome is disassembled into the 20S and 19S subcomplexes, mediated by the conformational switch of ECPAS. It is possible that additional ECPAS, which is usually sub-stoichiometrically associated with the 26S and 30S, can be recruited to the 19S complex under glucose-depleted conditions. The 19S-ECPAS complex may have an antagonistic role in the re-assembly between the 20S and 19S unless the ECPAS conformation is restored. Elevated levels of the free 20S proteasome facilitate the Ub-independent proteolysis of misfolded proteins, a strategy that may improve cell survival by alleviating ER stress and proteopathic stress.

glucose deprivation commence the 26S/30S disassembly. Proteomic studies have identified phosphorylated (Ser830 and Thr836) and SUMOylated (Lys1039) residues in ECPAS upon cellular stress.[31,32] How these PTMs contribute to the changes in ECPAS structures remains to be determined.

When cellular proteostasis is substantially perturbed by chronic stressors, such as starvation, oxidation, and proteasome inhibition, 26S proteasomes are often sequestered into various areas of the cell, such as the cytoplasm (e.g., PSGs), nucleus (starvation-induced proteasome assembly in the nucleus [SIPAN]), and perinuclear regions (aggresomes). These LLPS-mediated proteasome inclusion bodies are generally believed to be cytoprotective: either the impaired proteasomes are temporarily reserved or the concentrated proteasomes are more efficient at eliminating excess aberrant proteins. Intriguingly, the formation of PSGs is hardly observed in mammals upon glucose depletion, unlike in yeast or plants. Considering the high concentration of proteasomes in cells and the energy-costly *de novo* proteasome synthesis, it seems plausible that a large share of cellular proteasomes cannot be entirely sequestered in response to various stress conditions. Thus, 26S disassembly into the 20S and 19S proteasomes can provide a more rapid and pervasive adaptive cellular mechanism. It is possible that the disassembly process precedes autophagy induction under starvation conditions and the free 20S and autophagosomes largely have exclusive substrates. The two mechanisms are expected to complement each other at the later stage of stress responses: when total 26S proteasome activity is suppressed through sequestration or disassembly, induced autophagy will provide cells with energy and anabolic intermediates. When the stress is relieved, the 20S and 19S subcomplexes will efficiently re-associate for a highly controlled ATP-dependent and Ub-dependent proteolysis.

Eukaryotic cells contain a mix of 20S, 26S, and 30S proteasomes, while free 20S accounts for more than half of the total proteasomes.[33] In addition, more ~20% of cellular proteins are consistently degraded by the 20S proteasome.[34] However, it was originally believed that the 20S was an intermediate of the 26S proteasome assembling process or a latent enzymatic complex, which was released from the holoenzyme when ATP levels decreased.[35,36] The lack of an ATPase adaptor or Ub receptor has also concealed the proteolytic role of free 20S proteasomes; however, recent studies clearly demonstrated the functional importance of the 20S as a stand-alone protease through biochemical, structural, and mass-spectrometric analysis.[10] Archaea and certain bacteria contain a primordial form of the

20S-like protease complex that is only loosely associated with ATPase regulators and may also function independently.[37,38] We postulate that substrate hydrolysis at the proteolytic chamber may lead to conformational changes, as observed in the ClpP proteases.[39] This cycle confers a critical positive feedback for processive substrate degradation under stress conditions. Our current study supports the previous observations that such primordial proteolytic activity may be carried over into eukaryotic 20S proteasomes under certain stress conditions.

It is conceivable that the structural remodeling of 26S proteasomes under glucose-starvation conditions has strong pathological implications. During glucose depletion, it was mainly the free 20S proteasome, rather than the 26S or autophagy, that was responsible for the clearance of translationally misfolded proteins. The 20S proteasome more readily processes excessively produced misfolded proteins in a Ub-independent manner. In this context, one may consider the 20S as a "first-responder" or "emergency proteasome" to elevated levels of aggregate-prone misfolded polypeptides. Therefore, our data, together with those of previous findings, provide a framework for the universal proteasome quality control mechanism, suggesting that maintaining a functional 20S proteasome pool in the cell confers pro-survival properties in response to numerous proteopathic challenges. Chronic stress, which impairs the efficient 20S-26S proteasome conversion, may gradually lead to the development of proteopathies over time. It has been known for decades that bortezomib and other proteasome-targeting anticancer drugs initiate severe UPR or ER stress; however, the mechanisms underlying the anti-tumor effects are not completely understood. Based on our observations, we propose that a significant portion of these therapeutic effects may result from stabilizing the 26S holoenzyme complex and subsequently augmenting ER stress-mediated apoptosis.

Limitations of the study

Proteasomes are typically found in a mixture of 30S, 26S, 20S (and a few more) species across most cell types and species. The underlying factors that determine the distribution of these species remain unclear, although cells appear to respond to environmental cues and metabolic demands by altering the ratio of different proteasome configurations. Under typical growth conditions, the majority of detected proteasomes are the 26S/30S holoenzymes, which account for most of the peptidase activity in the cell. However, certain conditions, including glucose starvation, can induce their reversible disassembly into 19S and 20S subcomplexes. We, therefore, propose that there exists an equilibrium between holoenzymes (26S and 30S) and their subcomplexes (19S and 20S).

A somewhat confusing observation in the current study is the paucity of intact free 19S complexes detected in whole-cell extracts in contrast to the distinct presence of the 20S alongside the 26S and 30S proteasomes. Although our preliminary imaging evaluation identified few noticeable foci, it seems possible that a portion of the free 19S may be sequestered in PSGs, liquid droplets, or other loose aggregates that are not easily accessible by protocols that utilize soluble cell extracts, such as native gels. Alternatively, the free 19S subcomplex may be inherently unstable, at least relative to the 20S, and some of its constitutive or associated proteins are separated, which was in part visualized by our sucrose-gradient separation. Future experiments could be designed to investigate the stability of the 19S complex and its intracellular localization under typical and stressful conditions, which would provide further insight into the stability of the proteasome species.

The current study identifies ECAPS/Ecm29 as a sub-stoichiometric proteasome-interacting protein that appears to associate specifically with the 19S. Since we estimated ECPAS at ~5% of complexes on a molar ratio, and since knockout of ECPAS (in mammals) or Ecm29 (in yeast) displays similar proteasome distributions to their wild-type controls, we postulate that, under normal growth conditions, ECPAS does not play a significant role in the stability of 26S or the equilibrium between 26S/30S and 20S. However, the 19S and 20S disassemble with a conformation switch of ECPAS as a cue upon glucose depletion. This conformational change is likely to be correlated with the cellular redox status because other oxidative conditions (such as hypoxia, oxidative stress, or presence of free radicals) also display an increase of 20S-to-26S/30S ratio.

At present, we do not yet know the sequence of events; i.e., does the ECPAS conformational switch facilitate the disassembly of proteasome subcomplexes, or does the new conformation of ECPAS have a higher affinity for free 19S and therefore associate preferentially with the liberated 19S, thereby dampening the affinity of free 19S for free 20S? Since the stoichiometry of ECPAS on proteasomes is estimated to be sub-stoichiometric, and since our observations indicate a higher abundance of ECPAS associated with free 19S, it is possible that its conformational switch of ECPAS may not only facilitate the disassembly of proteasome subcomplexes but also stabilize the free 19S released from the 20S during glucose starvation. Therefore, in a follow-up work, it would be interesting to design experiments to evaluate the effect of ECPAS on proteasome re-assembly upon glucose recovery. Upon glucose recovery, ECPAS will resume its native conformation that either unblocks the attachment of the 19S to the 20S surface or lowers its affinity for 19S, facilitating the re-association between free 20S and 19S subcomplexes.

STAR★METHODS

Detailed methods are provided in the online version of this paper and include the following:

- KEY RESOURCES TABLE
- RESOURCE AVAILABILITY
  - Lead contact
  - Materials availability
  - Data and code availability
- EXPERIMENTAL MODEL AND STUDY PARTICIPANT DETAILS
  - Mammalian cell lines
  - Animals
  - Yeast strains
- METHOD DETAILS
  - Native gel electrophoresis and in-gel activity assay
  - Monitoring proteasomal activity via fluorogenic peptide substrates

- Generation of retrovirus for protein expression and stable cell lines
- Establishment of HEK293-PSMB2-HB$^{ECPAS-/-}$ cell lines
- Purification of human proteasomes
- Yeast proteasome analysis
- SDS-PAGE and gel staining
- Immunoblotting
- *In vitro* ubiquitination of Sic1^{PY} and its degradation assay with purified proteasomes
- Sucrose density gradient fractionation and size exclusion chromatography (SEC)
- Assessment of cell viability and intracellular ATP levels
- RNA isolation and RT-PCR
- RNA interference
- LC-MS/MS analysis with the iBAQ algorithm
- Computational modeling construction
- Assessment of intracellular glucose levels in xenograft mouse tumors

- QUANTIFICATION AND STATISTICAL ANALYSIS

SUPPLEMENTAL INFORMATION

Supplemental information can be found online at https://doi.org/10.1016/j.celrep.2023.112701.

ACKNOWLEDGMENTS

This work was supported by grants from the National Research Foundation of Korea (NRF; 2021R1A2C2008023 to M.J.L.; 2020R1A5A1019023 to D.H., M.J.L., and Y.T.K.; and 2020M3A9G7103933 to C.S.), the Korea Health Industry Development Institute and Korea Dementia Research Center (HU21C0071 to M.J.L.), the Gyeonggi-do Regional Research Center program (GRRC-Kyung Hee 2018[B03] to K.P.K.), and Israel Science Foundation grants (755/19 and 2512/18 to M.H.G.). M.J.L. also acknowledge financial support from the Interdisciplinary Research Initiatives Programs by SNU Medical School and SNU Boramae Medical Center (2021). All the authors gratefully acknowledge H.K. Song (Korea University) and K. Nam (UT Arlington) for technical assistance on structural analysis.

AUTHOR CONTRIBUTIONS

W.H.C., Y.Y., and I.B. were responsible for conducting most of the biochemical and cell-based experiments. I.B. and S.H.P. performed the CRISPR-Cas9-mediated ECPAS knockout. S.K. executed the gel filtration chromatography assays. S.L., J.S., I.B., J.J., and C.S. collaborated to undertake the structural modeling. O.K., K.P.K., and D.H. were responsible for performing quantitative LC-MS/MS analysis. T.C. generated the *ECPAS*$^{-/-}$ MEFs. Y.T.K. conducted the analysis of xenograft tumor tissues. S.L. and M.H.G. produced the yeast data and CycB degradation data. M.J.L., W.H.C., Y.Y., I.B., and M.H.G. performed manuscript writing, review, and editing. All authors provided critical review.

DECLARATION OF INTERESTS

The authors declare no competing interests.

Received: August 29, 2022
Revised: May 7, 2023
Accepted: June 9, 2023
Published: June 27, 2023

REFERENCES

1. Sontag, E.M., Samant, R.S., and Frydman, J. (2017). Mechanisms and Functions of Spatial Protein Quality Control. Annu. Rev. Biochem. *86*, 97–122.
2. Labbadia, J., and Morimoto, R.I. (2015). The biology of proteostasis in aging and disease. Annu. Rev. Biochem. *84*, 435–464.
3. Hamazaki, J., and Murata, S. (2020). ER-Resident Transcription Factor Nrf1 Regulates Proteasome Expression and Beyond. Int. J. Mol. Sci. *21*, 3683.
4. Dikic, I. (2017). Proteasomal and Autophagic Degradation Systems. Annu. Rev. Biochem. *86*, 193–224.
5. Kim, E., Park, S., Lee, J.H., Mun, J.Y., Choi, W.H., Yun, Y., Lee, J., Kim, J.H., Kang, M.J., and Lee, M.J. (2018). Dual function of USP14 deubiquitinase in cellular proteasomal activity and autophagic flux. Cell Rep. *24*, 732–743.
6. Finley, D. (2009). Recognition and processing of ubiquitin-protein conjugates by the proteasome. Annu. Rev. Biochem. *78*, 477–513.
7. Finley, D., Chen, X., and Walters, K.J. (2016). Gates, Channels, and Switches: Elements of the Proteasome Machine. Trends Biochem. Sci. *41*, 77–93.
8. Śledź, P., Unverdorben, P., Beck, F., Pfeifer, G., Schweitzer, A., Förster, F., and Baumeister, W. (2013). Structure of the 26S proteasome with ATP-gammaS bound provides insights into the mechanism of nucleotide-dependent substrate translocation. Proc. Natl. Acad. Sci. USA *110*, 7264–7269.
9. Abi Habib, J., De Plaen, E., Stroobant, V., Zivkovic, D., Bousquet, M.P., Guillaume, B., Wahni, K., Messens, J., Busse, A., Vigneron, N., and Van den Eynde, B.J. (2020). Efficiency of the four proteasome subtypes to degrade ubiquitinated or oxidized proteins. Sci. Rep. *10*, 15765.
10. Sahu, I., Mali, S.M., Sulkshane, P., Xu, C., Rozenberg, A., Morag, R., Sahoo, M.P., Singh, S.K., Ding, Z., Wang, Y., et al. (2021). The 20S as a standalone proteasome in cells can degrade the ubiquitin tag. Nat. Commun. *12*, 6173.
11. Lee, M.J., Lee, B.H., Hanna, J., King, R.W., and Finley, D. (2011). Trimming of ubiquitin chains by proteasome-associated deubiquitinating enzymes. Mol. Cell. Proteomics *10*. R110.003871.
12. VerPlank, J.J.S., and Goldberg, A.L. (2018). Exploring the Regulation of Proteasome Function by Subunit Phosphorylation. Methods Mol. Biol. *1844*, 309–319.
13. Choi, W.H., Yun, Y., Park, S., Jeon, J.H., Lee, J., Lee, J.H., Yang, S.A., Kim, N.K., Jung, C.H., Kwon, Y.T., et al. (2020). Aggresomal sequestration and STUB1-mediated ubiquitylation during mammalian proteaphagy of inhibited proteasomes. Proc. Natl. Acad. Sci. USA *117*, 19190–19200.
14. Peters, L.Z., Hazan, R., Breker, M., Schuldiner, M., and Ben-Aroya, S. (2013). Formation and dissociation of proteasome storage granules are regulated by cytosolic pH. J. Cell Biol. *201*, 663–671.
15. Yasuda, S., Tsuchiya, H., Kaiho, A., Guo, Q., Ikeuchi, K., Endo, A., Arai, N., Ohtake, F., Murata, S., Inada, T., et al. (2020). Stress- and ubiquitylation-dependent phase separation of the proteasome. Nature *578*, 296–300.
16. Uriarte, M., Sen Nkwe, N., Tremblay, R., Ahmed, O., Messmer, C., Mashtalir, N., Barbour, H., Masclef, L., Voide, M., Viallard, C., et al. (2021). Starvation-induced proteasome assemblies in the nucleus link amino acid supply to apoptosis. Nat. Commun. *12*, 6984.
17. Asano, S., Fukuda, Y., Beck, F., Aufderheide, A., Förster, F., Danev, R., and Baumeister, W. (2015). Proteasomes. A molecular census of 26S proteasomes in intact neurons. Science *347*, 439–442.
18. Pack, C.G., Yukii, H., Toh-e, A., Kudo, T., Tsuchiya, H., Kaiho, A., Sakata, E., Murata, S., Yokosawa, H., Sako, Y., et al. (2014). Quantitative live-cell imaging reveals spatio-temporal dynamics and cytoplasmic assembly of the 26S proteasome. Nat. Commun. *5*, 3396.

19. Laporte, D., Salin, B., Daignan-Fornier, B., and Sagot, I. (2008). Reversible cytoplasmic localization of the proteasome in quiescent yeast cells. J. Cell Biol. *181*, 737–745.

20. Leggett, D.S., Hanna, J., Borodovsky, A., Crosas, B., Schmidt, M., Baker, R.T., Walz, T., Ploegh, H., and Finley, D. (2002). Multiple associated proteins regulate proteasome structure and function. Mol. Cell. *10*, 495–507.

21. Gorbea, C., Goellner, G.M., Teter, K., Holmes, R.K., and Rechsteiner, M. (2004). Characterization of mammalian Ecm29, a 26 S proteasome-associated protein that localizes to the nucleus and membrane vesicles. J. Biol. Chem. *279*, 54849–54861.

22. Guerrero, C., Tagwerker, C., Kaiser, P., and Huang, L. (2006). An integrated mass spectrometry-based proteomic approach: quantitative analysis of tandem affinity-purified in vivo cross-linked protein complexes (QTAX) to decipher the 26 S proteasome-interacting network. Mol. Cell. Proteomics *5*, 366–378.

23. Choi, W.H., de Poot, S.A.H., Lee, J.H., Kim, J.H., Han, D.H., Kim, Y.K., Finley, D., and Lee, M.J. (2016). Open-gate mutants of the mammalian proteasome show enhanced ubiquitin-conjugate degradation. Nat. Commun. *7*, 10963.

24. Kleijnen, M.F., Roelofs, J., Park, S., Hathaway, N.A., Glickman, M., King, R.W., and Finley, D. (2007). Stability of the proteasome can be regulated allosterically through engagement of its proteolytic active sites. Nat. Struct. Mol. Biol. *14*, 1180–1188.

25. Wang, X., Chemmama, I.E., Yu, C., Huszagh, A., Xu, Y., Viner, R., Block, S.A., Cimermancic, P., Rychnovsky, S.D., Ye, Y., et al. (2017). The proteasome-interacting Ecm29 protein disassembles the 26S proteasome in response to oxidative stress. J. Biol. Chem. *292*, 16310–16320.

26. Sonn-Segev, A., Belacic, K., Bodrug, T., Young, G., VanderLinden, R.T., Schulman, B.A., Schimpf, J., Friedrich, T., Dip, P.V., Schwartz, T.U., et al. (2020). Quantifying the heterogeneity of macromolecular machines by mass photometry. Nat. Commun. *11*, 1772.

27. Iurlaro, R., Püschel, F., León-Annicchiarico, C.L., O'Connor, H., Martin, S.J., Palou-Gramón, D., Lucendo, E., and Muñoz-Pinedo, C. (2017). Glucose Deprivation Induces ATF4-Mediated Apoptosis through TRAIL Death Receptors. Mol. Cell Biol. *37*, e00479-16.

28. Yoshida, H., Matsui, T., Yamamoto, A., Okada, T., and Mori, K. (2001). XBP1 mRNA is induced by ATF6 and spliced by IRE1 in response to ER stress to produce a highly active transcription factor. Cell *107*, 881–891.

29. Urasaki, Y., Heath, L., and Xu, C.W. (2012). Coupling of glucose deprivation with impaired histone H2B monoubiquitination in tumors. PLoS One *7*, e36775.

30. Waku, T., Nakamura, N., Koji, M., Watanabe, H., Katoh, H., Tatsumi, C., Tamura, N., Hatanaka, A., Hirose, S., Katayama, H., et al. (2020). NRF3-POMP-20S Proteasome Assembly Axis Promotes Cancer Development via Ubiquitin-Independent Proteolysis of p53 and Retinoblastoma Protein. Mol. Cell Biol. *40*, e00597-19.

31. Impens, F., Radoshevich, L., Cossart, P., and Ribet, D. (2014). Mapping of SUMO sites and analysis of SUMOylation changes induced by external stimuli. Proc. Natl. Acad. Sci. USA *111*, 12432–12437.

32. Olsen, J.V., Vermeulen, M., Santamaria, A., Kumar, C., Miller, M.L., Jensen, L.J., Gnad, F., Cox, J., Jensen, T.S., Nigg, E.A., et al. (2010). Quantitative phosphoproteomics reveals widespread full phosphorylation site occupancy during mitosis. Sci. Signal. *3*, ra3. ra3.

33. Fabre, B., Lambour, T., Garrigues, L., Ducoux-Petit, M., Amalric, F., Monsarrat, B., Burlet-Schiltz, O., and Bousquet-Dubouch, M.P. (2014). Label-free quantitative proteomics reveals the dynamics of proteasome complexes composition and stoichiometry in a wide range of human cell lines. J. Proteome Res. *13*, 3027–3037.

34. Baugh, J.M., Viktorova, E.G., and Pilipenko, E.V. (2009). Proteasomes can degrade a significant proportion of cellular proteins independent of ubiquitination. J. Mol. Biol. *386*, 814–827.

35. Hendil, K.B., Kriegenburg, F., Tanaka, K., Murata, S., Lauridsen, A.M.B., Johnsen, A.H., and Hartmann-Petersen, R. (2009). The 20S proteasome as an assembly platform for the 19S regulatory complex. J. Mol. Biol. *394*, 320–328.

36. Livnat-Levanon, N., Kevei, É., Kleifeld, O., Krutauz, D., Segref, A., Rinaldi, T., Erpapazoglou, Z., Cohen, M., Reis, N., Hoppe, T., and Glickman, M.H. (2014). Reversible 26S Proteasome Disassembly upon Mitochondrial Stress. Cell Rep. *7*, 1371–1380.

37. Barthelme, D., and Sauer, R.T. (2012). Identification of the Cdc48*20S proteasome as an ancient AAA+ proteolytic machine. Science *337*, 843–846.

38. Majumder, P., and Baumeister, W. (2019). Proteasomes: unfoldase-assisted protein degradation machines. Biol. Chem. *401*, 183–199.

39. Kim, L., Lee, B.G., Kim, M., Kim, M.K., Kwon, D.H., Kim, H., Brötz-Oesterhelt, H., Roh, S.H., and Song, H.K. (2022). Structural insights into ClpP protease side exit pore-opening by a pH drop coupled with substrate hydrolysis. EMBO J. *41*, e109755.

40. Jumper, J., Evans, R., Pritzel, A., Green, T., Figurnov, M., Ronneberger, O., Tunyasuvunakool, K., Bates, R., Žídek, A., Potapenko, A., et al. (2021). Highly accurate protein structure prediction with AlphaFold. Nature *596*, 583–589.

41. Park, T., Baek, M., Lee, H., and Seok, C. (2019). GalaxyTongDock: Symmetric and asymmetric ab initio protein-protein docking web server with improved energy parameters. J. Comput. Chem. *40*, 2413–2417.

42. Park, H., Lee, G.R., Heo, L., and Seok, C. (2014). Protein loop modeling using a new hybrid energy function and its application to modeling in inaccurate structural environments. PLoS One *9*, e113811.

43. Heo, L., Lee, H., and Seok, C. (2016). GalaxyRefineComplex: Refinement of protein-protein complex model structures driven by interface repacking. Sci. Rep. *6*, 32153.

44. Haratake, K., Sato, A., Tsuruta, F., and Chiba, T. (2016). KIAA0368-deficiency affects disassembly of 26S proteasome under oxidative stress condition. J. Biochem. *159*, 609–618.

45. Wang, X., Chen, C.F., Baker, P.R., Chen, P.L., Kaiser, P., and Huang, L. (2007). Mass spectrometric characterization of the affinity-purified human 26S proteasome complex. Biochemistry *46*, 3553–3565.

46. Ziv, I., Matiuhin, Y., Kirkpatrick, D.S., Erpapazoglou, Z., Leon, S., Pantazopoulou, M., Kim, W., Gygi, S.P., Haguenauer-Tsapis, R., Reis, N., et al. (2011). A perturbed ubiquitin landscape distinguishes between ubiquitin in trafficking and in proteolysis. Mol. Cell. Proteomics *10*. M111.009753.

47. Dong, Y., Zhang, S., Wu, Z., Li, X., Wang, W.L., Zhu, Y., Stoilova-McPhie, S., Lu, Y., Finley, D., and Mao, Y. (2019). Cryo-EM structures and dynamics of substrate-engaged human 26S proteasome. Nature *565*, 49–55.

STAR★METHODS

KEY RESOURCES TABLE

REAGENT or RESOURCE	SOURCE	IDENTIFIER
Antibodies		
β-actin/ACTB	Sigma-Aldrich	Cat# A1978; RRID:AB_476692
PSMA4	Enzo Life Science	Cat# PW8115; RRID:AB_2171569
PSMA5	Invitrogen	Cat# PA5-17295; RRID:AB_10982616
PSMB5	Invitrogen	Cat# PA1-977; RRID:AB_2172052
PSMB6	Invitrogen	Cat# PA1-978; RRID:AB_2172197
PSMC2	Santa Cruz Biotechnology	Cat# sc-166972; RRID:AB_10611067
PSMC4	Abgent	Cat# AT3466a; RRID:AB_1554027
PSMD1	Santa Cruz Biotechnology	Cat# sc-514809
PSMD2	Invitrogen	Cat# PA527663; RRID:AB_2545139
PSMD11	Abclonal	Cat# A15306; RRID:AB_2762207
PSMD14	Abcam	Cat# ab109123;RRID:AB_10892165
LC3	Sigma-Aldrich	Cat# L7543; RRID:AB_796155
USP14	Invitrogen	Cat# PA5-30300; RRID:AB_2547774
RAD23A	Abclonal	Cat# A19884; RRID:AB_2862795
RAD23B	Abclonal	Cat# A20000; RRID:AB_2862908
VCP	Invitrogen	Cat# MA3-004; RRID:AB_2214638
TXNL1	Abclonal	Cat# A6322; RRID:AB_2766926
ECPAS	Invitrogen	Cat# PA3-035; RRID:AB_2130523
RPL23	Abclonal	Cat# A4292 RRID:AB_2765606
EEF2	Abclonal	Cat# A2068; RRID:AB_2764091
eEF1A1	Millipore	Cat# 05–235; RRID:AB_309663
RPL11	Abcam	Cat# ab79352; RRID:AB_2042832
RPS6	Cell Signaling Technology	Cat# 2217S; RRID:AB_331355
mTOR	Cell Signaling Technology	Cat# 2983S; RRID:AB_2105622
p-mTOR	Cell Signaling Technology	Cat# 5536S; RRID:AB_10691552
p-AKT	Cell Signaling Technology	Cat#4060S; RRID:AB_2315049
IRE1/ERN1	Cell Signaling Technology	Cat# 3294s; RRID:AB_823545
p-IRE1/p-ERN1	Invitrogen	Cat# PA1-16927; RRID:AB_2262241
T7	Bethyl Laboratories	Cat# PW9910; RRID:AB_67583
HSC70	Enzo Life Science	Cat# ADI-SPA-815-D; RRID:AB_2039279
HSP70	Enzo Life Science	Cat# ADI-SPA-810-D; RRID:AB_2039260
RPS14	Abclonal	Cat# A6727; RRID:AB_476755
RPL8	Abclonal	Cat# A10042; RRID:AB_2757564
eIF3e	Abcam	Cat# ab36766; RRID:AB_869604
HA	Biolegend	Cat# 901501; RRID:AB_2565006
flag	Invitrogen	Cat# PA1-984B; RRID:AB_347227
Chemicals, peptides, and recombinant proteins		
MG132	AG scientific	Cat# M-1157
MLN7243	Cayman Chemical	Cat# 30108
BafilomycinA1	Cayman Chemical	Cat# 11038
Puromycin	Cayman Chemical	Cat# 13884
suc-LLVY-AMC	Bachem	Cat# I-1395
DMEM	Wellgene	Cat# LM001-05
Glucose-free DMEM	Wellgene	Cat# LM001-79

(*Continued on next page*)

Continued

REAGENT or RESOURCE	SOURCE	IDENTIFIER
RPMI-1640	Wellgene	Cat# LM011-01
Glucose-free RPMI-1640	Wellgene	Cat# LM011-60
Dialyzed FBS	Gibco	Cat# A3382001
Critical commercial assays		
Coomassie Protein Assay Reagent	Thermo-Fisher	Cat# 23200
Picoprobe Glucose Assay Kit	Abcam	Cat# ab169559
ATP determination kit	Invitrogen	Cat# A22066
NuPAGE^{TM} 3–8% Tris-Acetate Protein Gels	Thermo-Fisher	Cat# EA0375BOX
Lipofectamine RNAiMAX	Invitrogen	Cat# 13778075
Deposited data		
iBAQ-MS analysis of purified proteasome	This study, ProteomeXchange	PXD034609
Experimental models: Cell lines		
Human: HEK293	KCLB	Cat# 21573
Human: HEK293-PSMB2-HB	This study	N/A
Human: HEK293-PSMD14-HB,	This study	N/A
Human: HEK293-PSMB2-HB$^{ECPAS-/-}$	This study	N/A
Human: HeLa	KCLB	Cat# 10002
Mouse: MEFs	Dr. Tomoki Chiba (University of Tsukuba)	N/A
Mouse: *ECPAS*$^{-/-}$ MEFs	Dr. Tomoki Chiba (University of Tsukuba)	N/A
Human: A549	KCLB	Cat# 10185
Human: A549-PSMB5-HB	This study	N/A
Human: HEK293 GP2	Takara Bio	Cat# 631458
Experimental models: Organisms/strains		
SUB62 WT (ura3-52, his3-200, leu2-3,112, lys2-801, trp1-1, gal)	Dr. Michael H. Glickman (Technion–Israel Institute of Technology)	N/A
SUB62 Δecm29:TRP1	Dr. Michael H. Glickman (Technion–Israel Institute of Technology)	N/A
Mouse: 7-week-old NOD/SCID mice	The Jackson Laboratory	Cat# 001303
Oligonucleotides		
All oligonucleotides used in this study can be found in Table S5	This study	N/A
Recombinant DNA		
Plasmid: pME-Flag-ECPAS	Dr. Tomoki Chiba (University of Tsukuba)	N/A
Plasmid: pCS-6-SmaSh-CyclinB1-WT	Dr. Michael H. Glickman (Technion–Israel Institute of Technology)	N/A
Plasmid: pCS-6-SmaSh-CyclinB1-K0	Dr. Michael H. Glickman (Technion–Israel Institute of Technology)	N/A
Plasmid: VSV-G	Addgene	Cat# 14888
Plasmid: pQCXIP-PSMB5-HB	This study	N/A
Software and algorithms		
ImageJ	NIH	1.53s
Magellan 7	Tecan	7
GraphPad Prism	GraphPad	ver. 9.3.1

(*Continued on next page*)

Continued

REAGENT or RESOURCE	SOURCE	IDENTIFIER
AlphaFold	Jumper et al.[40]	N/A
GalaxyTongDock	Park et al.[41]	N/A
GalaxyLoop	Park et al.[42]	N/A
GalaxyRefineComplex	Heo et al.[43]	N/A

RESOURCE AVAILABILITY

Lead contact

Further information and requests for reagents may be directed to, and will be fulfilled by, the Lead Contact, Min Jae Lee (minjlee@snu.ac.kr).

Materials availability

All unique reagents generated in this study are available from the lead contact with a completed Materials Transfer Agreement.

Data and code availability

The proteomics data have been deposited to the ProteomeXchange Consortium with the dataset identifier PRIDE: PXD034609. Please refer to key resources table. This paper does not report original code. Any additional information required to reanalyze the data reported in this paper is available from the lead contact upon request.

EXPERIMENTAL MODEL AND STUDY PARTICIPANT DETAILS

Mammalian cell lines

Mammalian cells used in this study, including HEK293, HEK293-PSMB2-HB, HEK293-PSMD14-HB, HEK293-PSMB2-HB-ΔECPAS, HeLa, +/+ MEFs, and *ECPAS*$^{-/-}$ MEFs[44] are summarized in this paper's key resources table. The cells were cultured in DMEM, whereas A549 and A549-PSMB5-HB cells were grown in RPMI-1640 media. All culture media supplemented with heat-inactivated 10% fetal bovine serum, 100 units/mL penicillin/streptomycin, and 2 mM L-glutamine. Cells were routinely tested for mycoplasma contamination. For glucose depletion, cells were washed twice with glucose-free DMEM and cultured in glucose-free DMEM supplemented with 10% dialyzed FBS (A3382001, Gibco), 100 units/mL penicillin/streptomycin, and 2 mM L-glutamine. All the reagents were treated to the cells as below unless otherwise described: MG132 (10 μM; M-1157, AG scientific), bafilomycin A1 (100 nM; 11038, Cayman Chemical), MLN7243 (1 μM, 30108, Cayman Chemical), Cycloheximide (80 μg/mL; 14126, Cayman Chemical), and puromycin (250 ng/mL to 10 μg/mL; 13884, Cayman Chemical).

Animals

Mice were housed in a facility fully accredited by the Institutional Animal Care and Use Committee (IACUC) of Seoul National University. For the assessment of 26S/20S proteasome ratios in a tumor, A549 cells (5×10^6 cells) were suspended in 1 mL of 1:1 mixture of PBS and matrigel, and 100 μL aliquot was subcutaneously injected into the right flank region of 7-week-old NOD/SCID mice (The Jackson Laboratory) with a 26-gauge syringe. The mice were sacrificed after 2 or 6 weeks post-implantation, and the tumor tissues, lungs, and other organs were removed for subsequent biochemical analyses.

Yeast strains

SUB62 WT (ura3-52, his3-200, leu2-3,112, lys2-801, trp1-1, gal), SUB62 Δecm29TRP1. Cultures were grown in Standard YEP medium (1% yeast extract, 2% Bacto Peptone) supplemented with 2% dextrose (YPD). Yeast cells were grown exponentially in 5 mL YPD medium for 24h (the logarithmic phase) or for 9 days (the stationary phase and starvation period).

METHOD DETAILS

Native gel electrophoresis and in-gel activity assay

Native gel analysis was performed as previously described.[13] WCLs and chromatography fractions were prepared with buffer A and buffer C (proteasome SEC buffer; 50 mM NaH_2PO_4 pH 7.5, 10 mM NaCl, 5 mM $MgCl_2$, 5 mM ATP, 1 mM DTT, and protease inhibitor cocktails), respectively. Samples were resolved by NuPAGE 3–8% Tris-Acetate Protein Gels (Thermo-Fisher) at 150 V for 3–4 h. Gels were incubated in buffer D (in-gel activity assay buffer; 20 mM Tris, 1 mM ATP, 5 mM $MgCl_2$) with proteasome fluorogenic substrate (100 μM suc-LLVY-AMC) for visualizing proteasome complexes. The addition of 0.02% SDS during in-gel hydrolysis assay activated and visualized the 20S proteasome. After the in-gel hydrolysis assay, separated protein complexes were transferred to PVDF membranes for subsequent immunoblotting analysis.

Monitoring proteasomal activity via fluorogenic peptide substrates

Hydrolysis of the fluorogenic-peptide substrates suc-LLVY-AMC (7-amino-4-methylcoumarin; Bachem) was quantified to determine the proteolytic activity of proteasomes, as previously described.[23] Briefly, the fluorogenic-peptide substrate hydrolysis assay was carried out with 0.5 nM purified proteasome and 12.5 μM of suc-LLVY-AMC in buffer E (proteasome activity assay buffer; 50 mM Tris-HCl pH 7.5, 1 mg/mL BSA, 1 mM EDTA, 1 mM ATP, and 1 mM DTT). Proteasome activity was monitored by measuring free AMC fluorescence in a black 96-well plate on a TECAN infinite m200 fluorometer.

Generation of retrovirus for protein expression and stable cell lines

Stable cell lines such as A549-PSMB5-HB for proteasome purification were generated by retrovirus transduction and antibiotics selection, largely as previously described.[45] Briefly, plasmids expressing pQCXIP-PSMB5-HB and VSV-G were co-transfected into a 293 GP2 cell line. After transfection for 48 h, the medium containing the retrovirus was collected and mixed with 5 μg/mL polybrene to transduce A549 cells and then gradually selected with puromycin (1–3 μg/mL) to establish stable cell lines.

Establishment of HEK293-PSMB2-HB$^{ECPAS-/-}$ cell lines

sgRNA sequences targeting *ECPAS* (5′-GCACAGCGAACTCTCATGGAGG-3′) were identified using the CRISPR RGEN Tools (http://www.rgenome.net/) by screening exonic regions of *ECPAS* (RefSeq: NC_000009.12). The sgRNAs with overhangs for BbsI sites were annealed using two primers, 5′-caccgGCACAGCGAACTCTCATGG-3′ and 5′-aaacCCATGAGAGTTCGCTGTGCc-3′, and ligated into digested pSpCas9(BB)-2A-GFP with BbsI by T4 DNA ligase. HEK293-PSMB2-HB cells were transfected with 5 μg of the cloned plasmid using Lipofectamine 3000 (Invitrogen). After 48 h incubation, cells were trypsinized, and GFP-positive cells were sorted by fluorescence-assisted cell sorting (FACS, BD AriaIII). To isolate single clones, FACS-sorted cells were seeded in 96-well culture plates with low density (~0.5 cells per well), and the knockout efficiency of each clone was later confirmed by genotyping with Sanger sequencing and immunoblotting against ECPAS.

Purification of human proteasomes

Human proteasomes were isolated by affinity purification from a stable HEK293 and A549 cell lines expressing biotin-tagged human PSMB2, PSMB5, and PSMD14 as previously described.[23] The cells were harvested with buffer A (proteasome lysis buffer; 25 mM Tris-HCl pH 7.5, 10% glycerol, 5 μM $MgCl_2$, 1 mM ATP, 1 mM DTT, and protease inhibitor cocktail) and homogenized with Dounce homogenizer. After that, the lysates were centrifuged at 16,000 × g for 15 min at 4°C. Next, the supernatants were incubated with streptavidin magnetic beads for 16 h at 4°C. The beads were washed twice with buffer A and once with buffer B (TEV cleavage buffer; 50 mM Tris-HCl pH 7.5 containing 1 mM ATP and 10% glycerol). Next, the proteasomes were eluted from the magnetic resin by incubating with TEV protease (Invitrogen) in buffer B containing 1 mM ATP for 1 h 30 min at 30°C. Then, the eluted human proteasomes were concentrated with Amicon Ultra-0.5 centrifugal filter units (Millipore).

Yeast proteasome analysis

Yeast cells were centrifuged at 3000 rpm for 2 min, and the pellet was resuspended in 2-fold volume of ATP-depleted buffer A (1 M Tris, pH 7.4, 10% glycerol, 1 M $MgCl_2$). Cell were lysed using buffer A (0.5 M ATP and 1 M DTT added), 2-fold volume of glass beads was added to the tubes and the lysates underwent 5–6 intervals of 1 min vortex followed by 1 min in ice. The resultant supernatant was clarified by further centrifugation at 13,000 rpm for 30 min at 4°C. The final supernatant was used immediately as the crude native extract. The protein concentration was determined by the method of Bradford and all gels were normalized to protein content. For nondenaturing PAGE resolving of 30S\26S\20S proteasomes, protein crude extract samples were resolved by 4% nondenaturing Tris-borate (pH 8.0) PAGE. The gels were then incubated in 10 mL of 0.1 mM suc-LLVY-AMC in buffer A for 10 min at 30°C. Proteasome bands were visualized upon exposure to UV light (360 nm). For immunochemical identification of the 19S, protein samples were resolved on 10% SDS-PAGE followed by immunoblotting analysis using antibodies against Rpn1 (1:5,000) and Rpn5 (1:5,000).

SDS-PAGE and gel staining

Cultured cells were washed twice with PBS, and whole-cell lysates were prepared in RIPA buffer supplemented with a protease inhibitor cocktail. For SDS-PAGE, lysates mixed with sample buffer (final 6.3% glycerol, 80 mM Tris-HCl pH 6.8, 62.5 μg/mL bromophenol blue, 10 mg/mL SDS, and 5% 2-mercaptoethanol) and denatured at 85°C for 10 min. After the running step, relatively small amounts of proteins were visualized by silver staining (K14040D, Koma Biotech) as the manufacturer's guideline. Briefly, gels were fixed for 20 min or overnight in a fixing solution (40% (v/v) ethanol, 10% acetic acid, and 40% deionized water). They were then rinsed with a second fixing solution (50% ethanol in deionized water) and incubated with a sensitizing solution. After several washing steps with ultrapure water, gels were incubated in staining solution for 20 min and then in developing solution until the desired intensity was obtained. Image development was terminated by adding acetic acid (final 2%) and gentle agitation for 10 min.

Immunoblotting

For immunoblotting, separated proteins by SDS-PAGE were transferred to polyvinylidene difluoride (PVDF) membrane. The membranes were blocked with 5% nonfat milk in TBS-T (20 mM Tris-HCl pH 7.5, 150 mM NaCl, and 0.1% (w/v) Tween 20) solution and incubated with primary antibody. Antibodies used in this study are summarized in key resources table. The membranes were

then washed with TBS-T solution several times and followed by a horseradish peroxidase-conjugated anti-rabbit IgG or anti-mouse IgG antibody. After antibody incubation, bands were visualized via chemiluminescence, imaged, and quantified. ImageJ software was used to quantify bands intensity from independently replicated experiments more than three times, and statistical analysis was performed using GraphPad Prism V5 software (GraphPad Software). Results were evaluated to be significant with 95% confidence (p value less than 0.05).

In vitro ubiquitination of Sic1^{PY} and its degradation assay with purified proteasomes

Polyubiquitinated Sic1 with PY motif (Ub-Sic1^{PY}) was prepared as previously described.[23] Briefly, the Ub conjugation reaction was conducted with 10 pmol Sic1^{PY}, 2 pmol Uba1, 5 pmol Ubc4, 5 pmol Rps5, and 1.2 nmol ubiquitin in buffer F (ubiquitination reconstitution buffer; 50 mM Tris-HCl pH 7.4, 100 mM NaCl, 1 mM DTT, 2 mM ATP, and 10 mM $MgCl_2$) for 4 h and 25°C. For Ub-Sic1 degradation assay, purified human proteasomes (5 nM) under normal or glucose-depleted conditions were incubated with 20 nM of Ub-Sic1^{PY} in buffer E. Ub-Sic1^{PY} degradation was monitored by SDS-PAGE/immunoblotting using anti-T7 antibodies (Millipore).

Sucrose density gradient fractionation and size exclusion chromatography (SEC)

For sucrose-gradient ultracentrifugation, +/+ and *ECPAS*$^{-/-}$ MEFs extracts were homogenized with 1 mL of buffer C and centrifuged. After harvesting, the soluble fractions were loaded on top of a pre-established sucrose gradient (12 mL, 10–30%) and centrifuged at 312,000 × g in a Beckman SW-41 Ti rotor for 16 h at 4°C. After that, the gradients were manually fractionated into 300 μL fractions from top to bottom. For SEC, HeLa WCLs were centrifuged twice at 18,000 × g for 30 min at 4°C, loaded (11 mg by protein) onto a column, and eluted with buffer C. SEC was carried out on a Superose 6 Increase 10/300 GL column by fast protein liquid chromatography (ÄKTA; GE Healthcare); 0.25 mM fractions were collected, and 10% glycerol was added to each fraction.

Assessment of cell viability and intracellular ATP levels

Cell viability assays were performed using a modified 3-(4, 5-dimethylthiazol-2-yl)-2, 5-diphenyltetrazolium bromide (MTT) assay. Briefly, MTT solution was added to the cell culture media and incubated for 3 h at 37°C to form blue MTT-formazan products, which were assessed by measuring absorbance measurement (570 nm for test and 630 nm for reference wavelength). Cellular ATP concentration was measured using a coupled luciferin-luciferase reaction with the ATP determination kit (A22066, Invitrogen). Briefly, cells were plated in 6-well plates in equal densities. After treatment, cells were washed twice with PBS and then scrapped with buffer G (ATP assessment buffer; 25 mM Tris-HCl pH 7.5, 0.1% Triton X-100). Cells were homogenized with a 26G 1/2 needle attached to a 1 mL syringe and incubated for 15 min on ice. The samples were centrifuged at 13,000 rpm for 10 min at 4°C in a tabletop centrifuge. Samples (10 μL) were mixed with 90 μL of ATP reaction solution and rapidly assessed using a luminometer (TECAN Infinite 200 PRO)

RNA isolation and RT-PCR

Total RNA was isolated from either A549 or MEF cells using TRIzol-reagents and additional purification using RNeasy mini-columns (Qiagen) with on-column DNase I treatment. cDNA samples were prepared using two micrograms of total RNA by reverse transcription (RT)-PCR (Accupower RT-pre-mix, Bioneer). Quantitative RT-PCR reactions were conducted with 1/20 diluted cDNA, SYBR qPCR master mixture (Kapa Biosystems, USA) as the reporter dye, and 10 pmol of primers to detect mRNA expression of specific genes. Primer sequences used in this study are summarized in Table S5. Each mRNA level was normalized to that of *GAPDH*. Unpaired Student's t-tests were performed to evaluate the results, where p values of less than 0.05 were considered statistically significant.

RNA interference

The siRNAs were synthesized by Genolution. The siRNA duplex used in this study are summarized in Table S5. The siRNA duplex target sequences within the 3′ untranslated regions (3′-UTR) of human *ECPAS* mRNA. siRNA duplexes (siRNA B and C) were transfected into HEK293-PSMB2-HB cells using RNAiMAX (Invitrogen) dissolved in Opti-MEM (Invitrogen), following the manufacturer's protocols. The final concentration of siRNA for transfection was 20 nM. After 24 h, cells were trypsinized, suspended in the transfection mixture, and re-plated. On the following day, cells were transfected again with the siRNA duplexes and grown for an additional 48 h for an effective knockdown.

LC-MS/MS analysis with the iBAQ algorithm

The label-free, quantitative LC-MS/MS analysis with the iBAQ algorithm was performed, mainly as previously described,[13] with modifications in data analysis. Briefly, the iBAQ values obtained from biological triplicates in each condition were normalized to the average values of PSMB2 subunits from biological replicates. To identify proteasome-associating proteins whose interactions were significantly altered upon glucose starvation, we first selected preliminary differentially associated proteins (DAPs; >1.5-fold changes and <0.05 absolute p values) between glucose-deprived and control conditions. Next, using the log2-iBAQ values, we estimated the empirical null distribution (i.e., a protein is not differentially expressed between two conditions) of t-statistic values between the two conditions by performing random permutations of all six samples (three normal and three glucose-depleted conditions) 1,000 times. We then computed adjusted p values using the estimated empirical distribution. We finally selected the DAPs as the proteins with adjusted p values <0.05 and absolute log2-fold-changes >1 (2-fold). In addition, we included the proteins detected more than once in one sample group alone as the DAPs.

To obtain stoichiometric abundance of ECPAS compared to the proteasome, active proteasome bands from 4% native gel were excised under UV light after incubating them with Suc-LLVY-AMC substrate and collected into clean tubes. The proteins were fixed using rapid Coomassie stain after an overnight incubation, the stain was removed, and gel slices were washed several times with ddH2O. The slices were reduced with 10 mM DTT at 60°C for 30 min, modified with 100 mM iodoacetamide in 10 mM ammonium bicarbonate at room temperature for 30 min, and trypsinized in 10 mM ammonium bicarbonate containing Sequencing-grade modified trypsin at a 1:50 enzyme-to- substrate ratio, overnight at 37°C as described before.[46]

Computational modeling construction

In silico structure modeling of the ECPAS-26S proteasome complex was performed using AlphaFold[40] and GalaxyTongDock,[41] based on the available structure of the 26S proteasome in the substrate-accepting state (PDB: 6MSB,[47]) and the predicted structure of ECPAS (https://alphafold.ebi.ac.uk/entry/Q5VYK3). The AlphaFold model has a high confidence level in terms of the overall structure, with a median pLDDT of 88.41. For the initial-stage construction of ECPAS-bound 19S structures, the interface option of GalaxyTongDock was used to favor previously proposed interaction partners of ECPAS, including subunits PSMD2/Rpn1, PSMD4/Rpn10, PSMC2/Rpt1, and PSMC3/Rpt5.[20,25] Two different modeling with PSMD and PSMC subunits resulted in two different conformational states, termed ‘‘assembled’’ and ‘‘disassembled’’ states, respectively. The undefined loop structure in the middle of PSMD4 (amino acids 192–323) was filled with a predicted structure generated by AlphaFold-Multimer and GalaxyLoop.[42] Energy minimization, segment connection, side-chain repacking, and additional linker modeling were performed by in-house GALAXY tools for the predicted complexes to retain no disaccorded structure, such as steric clashes at the interface and mismatches from the experimentally identified proteasome structures. For further refinement, the models were equilibrated by the GalaxyRefineComplex program which uses a linear combination of energy functions including physics-based, knowledge-based, and restraint energy terms.[43]

Assessment of intracellular glucose levels in xenograft mouse tumors

Cellular glucose concentration was measured using the Picoprobe Glucose Assay Kit (ab169559, Abcam) according to the manufacturer’s protocol. Briefly, xenograft mouse tumor tissues were homogenized with 100 μL of Glucose Assay Buffer and centrifuged at 13,000 rpm for 5 min in a tabletop centrifuge. The supernatant of lysates was assessed for protein content using the Coomassie Protein Assay Reagent (23200, Thermo Fisher Scientific) and spin filtered through Amicon Ultra-0.5 centrifugal filter units (10 kDa MWCO, Millipore) to remove proteins and various enzymes. The filtered lysates were loaded at 2 μg protein per well in a 96 black-well plate, and a reaction mixture was added. After incubation for 30 min at 37°C, the fluorescence signal was measured at Ex/Em 535/587 nm.

QUANTIFICATION AND STATISTICAL ANALYSIS

Statistical significance of differences between various groups was determined by two-tailed Student’s *t*-test or one-way ANOVA followed by the Bonferroni *post hoc* test for most data (GraphPad Prism, ver. 9.3.1). Differences were considered significant at $p < 0.05$.